NASA Technical Memorandum 84375

(NASA-TM-84375) AN EXPERIMENTAL DOCUMENTATION OF TRAILING-EDGE FLOWS AT HIGH REYNOLDS NUMBER (NASA) 48 p HC A03/MF A01 CSCL 20D

N84-10498

Unclas G3/34 42252

An Experimental Documentation of Trailing-Edge Flows at High Reynolds Number

P.R. Viswanath, J.W. Cleary and H.L. Seegmiller

August 1983

National Aeronautics and Space Administration

NASA Technical Memorandum 84375

An Experimental Documentation of Trailing-Edge Flows at High Reynolds Number

P. R. Viswanath, Joint Institute for Aeronautics and Acoustics, Stanford University, Stanford, California
J. W. Cleary and H. L. Seegmiller, Ames Research Center, Moffett Field, California

NASA
National Aeronautics and Space Administration

Ames Research Center
Moffett Field, California 94035

NOMENCLATURE

A,B	calibration constants
c_f	wall skin-friction coefficient
I	electric current
k	kinetic energy of turbulence, $1/2(\langle u'^2 \rangle + \langle v'^2 \rangle + \langle w'^2 \rangle)$
L	model length
M	Mach number
P_T	total pressure
p	static pressure
R	gauge resistance or model leading-edge radius (fig. 1)
Re	unit Reynolds number per meter
T	temperature
u	velocity component in x-direction
u^+	law-of-the-wall velocity coordinate in x-direction
$\langle u'^2 \rangle$	mean square of velocity fluctuation in x-direction
$\langle v'^2 \rangle$	mean square of velocity fluctuation in y-direction
$\langle w'^2 \rangle$	mean square of velocity fluctuation in z-direction
x	streamwise coordinate parallel to model centerline measured from model trailing edge
y	vertical coordinate normal to model centerline measured from model surface and in the wake from the model trailing edge
y^+	law-of-the-wall distance coordinate
z	spanwise coordinate parallel to model trailing edge measured from tunnel midspan
α	flap-deflection angle
δ	boundary-layer thickness
δ^*	displacement thickness
θ	momentum thickness
μ	molecular viscosity

ρ	density
τ	shear stress

Subscripts:

e	boundary-layer edge conditions
g	gauge
L	based on model length
n	nominal free-stream conditions
o	reference conditions
T	total
t	turbulent
w	wall

AN EXPERIMENTAL DOCUMENTATION OF TRAILING-EDGE FLOWS AT HIGH REYNOLDS NUMBERS

P. R. Viswanath,* J. W. Cleary, and H. L. Seegmiller

Ames Research Center

SUMMARY

Experiments documenting attached trailing-edge and near-wake flows at high Reynolds numbers are described. A long, airfoil-like model was tested at subsonic and low transonic Mach numbers, and both symmetrical and asymmetrical flows with pressure gradients upstream of the trailing edge were investigated. Model surface pressures and detailed mean and turbulence flow qualities were measured in the vicinity of the trailing edge and in the near-wake. The data obtained are presented mostly in tabular form; they are of sufficient quality and detail to be useful as test cases in assessing turbulence models and calculation methods.

INTRODUCTION

In recent years, there has been growing interest in understanding and predicting airfoil trailing-edge flows, particularly at transonic speeds. Proper modeling of the flow in the vicinity of the trailing edge and in the near-wake is quite important in predicting airfoil performance (refs. 1 and 2). Moreover, this problem provides a good example of interacting turbulent shear layers which are not well understood.

At Ames Research Center, two-dimensional, trailing-edge flows at high Reynolds numbers have been investigated for the purpose of assessing the importance of turbulence modeling and viscous-inviscid interaction effects in trailing-edge flows. Detailed experiments on relatively simple aft-body shapes have been conducted in which symmetrical and asymmetrical trailing-edge flows, with pressure gradients upstream of the trailing-edge, have been studied at subsonic and low transonic Mach numbers. An additional objective of these experiments has been to provide a data base for use in evaluating turbulence models and calculation methods. In fact, the three flows described in this report were selected as test cases at a recent Stanford conference (ref. 3) on complex, turbulent flows.

Results from these experiments, along with comparisons of both boundary-layer and Navier-Stokes solutions employing different turbulence models, have already been published (refs. 4 and 5). In this report, we describe the experiments in detail; most of the data are presented in tabular form, but some are also shown graphically to illustrate the flow field and the variation of flow quantities.

---

*Research Associate, Joint Institute for Aeronautics and Acoustics, Stanford University, Stanford, California.

EXPERIMENTS

Test Facility

The experiments were conducted in the 38.1- by 25.4-cm (15- by 10-in.) high Reynolds number blowdown facility at Ames Research Center (fig. 1(a)). In that facility, the tunnel Mach number can be varied in discrete steps by appropriately choosing the choke inserts located downstream of the test section. Finer control of Mach number is achieved through use of a translating wedge located near the choke insert.

Model Configuration

The model configuration, which spans the test section, is made up of two parts: (1) a forebody, which is a flat plate 56.75 cm long and 2.54 cm thick with a 24.51-cm tapered forward section that has a leading edge radius of 0.52 cm (fig. 1(b)); and (2) an aft body flap with a sharp trailing edge, which is 11.63 cm long and has an included angle of 12.5° (fig. 1(b)). The flap can be deflected to angles up to ±20°. The above model configuration was chosen because of the following advantages: (1) it provides a thick and fully developed turbulent boundary layer, which is desirable for modeling studies; (2) the flap can be deflected to impose different pressure gradients on the flap boundary layer; and (3) the relatively long length of the model combined with the high stagnation pressures available with the facility gives high Reynolds numbers, a unique feature of the present experiment.

Flows Studied and Test Conditions

The tests on symmetrical trailing-edge flows were conducted at two nominal free-stream Mach numbers,[1] M_n, of 0.4 and 0.7; the asymmetrical flow was studied only at a Mach number of 0.4. The asymmetry was produced by deflecting the flap downward by an angle α of 6.25°. With this flap deflection, the lower surface of the flap was aligned with the lower surface of the flat plate, providing a zero pressure gradient, turbulent boundary-layer flow on the lower surface. Only the turbulent boundary layer on the upper surface of the flap experienced pressure gradients before reaching the trailing edge.

The free-stream Reynolds number based on model length, Re_L, was varied between 9×10^6 and 60×10^6 over the range of Mach numbers and stagnation pressures P_T of the test. Because the influence of Reynolds number on model surface pressures was found to be small, all the detailed flow-field measurements were made only at the moderately high stagnation pressure of 275 kN/m^2. The nominal total temperature T_T of the tests was 480°R. The total temperature variation about the nominal value was within ±10°F during different runs and over the period the tests were made. The total pressure was held constant within ±1.7 kN/m^2 for different runs.

---

[1]The nominal Mach number quoted refers to the nearly constant downstream tunnel Mach number estimated (for $x > 30$ cm) from the measured tunnel-wall pressures. Free-stream Mach number for each flow is not known precisely since the model leading edge is close to the entrance section (fig. 1(a)), but it is likely to be slightly less than the value quoted above in view of the relatively smaller boundary-layer displacement-thickness effects at the entrance location.

The flow conditions for the three different flows documented were as follows:

M_n	Re_L	α, deg
0.4	24.3×10^6	0
0.7	36.6×10^6	0
0.4	24.3×10^6	6.25

Surface Measurements

The flat-plate model had 68 static pressure orifices, 0.075-cm i.d., most of which were located on the centerline of the model on the upper and lower surfaces. Spanwise static pressure orifices, in the flat plate and flap region, corresponding to specific streamwise stations on the centerline, made it possible to assess the spanwise uniformity of surface pressures. Static-pressure orifices at intervals of 10 cm were also provided on the tunnel top and bottom walls in the region of the model, as well as downstream up to a distance of 45 cm. The pressures were measured with strain-gauge pressure transducers; which were calibrated before each tunnel run.

Wall shear-stress measurements on the flap were made using hot-wire surface gauges embedded in an alternative flap. More detailed information on these gauges is available in references 6 and 7. There were six gauges on each side of the flap. Each gauge consisted of a 5-μm-diam tungsten wire and a thermocouple located downstream of the hot wire for recording wall temperature. The heat loss from the wire is related to the local wall shear-stress through the relation

$$\frac{I^2R}{T_g - T_w} = A(\rho\mu\tau)_w^{1/3} + B$$

The gauges were calibrated using the fully developed turbulent boundary layer on the upper surface of the flat-plate forebody and the flap ($\alpha = -6.25°$, so that it formed a continuous surface with the forebody) at each Mach number. During the calibration tests, an extension plate was attached to the flap to extend the boundary-layer flow of the flat plate beyond the trailing edge. This plate was used mainly to avoid the possible upstream influence of the trailing edge in the absence of the extension plate. Wall shear-stress results obtained from a boundary-layer code employing the Wilcox-Rubesin two-equation turbulence model (ref. 8) were used for the calibrations. As reported in reference 9, the calibration curve was found to be nonlinear for large values of $(\rho\mu\tau)_w^{1/3}$ and the coefficient B was dependent on T_w. A procedure similar to that described in reference 9 was used to obtain the calibration curve for each gauge.

Flow-Field Measurements

Flow-field measurements were made using a two-color, laser-Doppler velocimeter (LDV), as well as conventional pitot and static probes. Two static-pressure probes, one with an ellipsoidal and the other with a conical nose, were used, with appropriate calibrations for each probe. Pitot- and static-probe pressures were measured with strain-gauge-type pressure transducers.

A schematic of the LDV optical arrangement is shown in figure 2. The two-component system employed a 4-W argon laser with a dispersing prism to obtain beams of 488- and 514.5-nm wavelength. The two beams were split, rotated ±45°, and intersected in the flow field at a location at the midspan of the model. The forward-scattered light, from particles passing through the volume formed by the intersection of the four beams, was optically collected and transmitted to photomultiplier tubes. The probe region was approximately 0.3 mm in diameter and about 3 mm long in the spanwise direction. Bragg cells were used to enable the system to detect velocity direction by causing the fringes within the stationary measuring region to move downstream at the Bragg frequency of 40 MHz. Vertical, axial, and chordwise movement of the probe region during surveys was accomplished by remotely positioning the optical bench that supported the laser and optics.

A two-channel counter system measured the velocity of particles passing through the probe region. Pulse-stretching, velocity consistency checks on the basis of particles crossing five and eight fringes, and signal-amplitude limiting were employed. Doppler signals were processed by the counters and passed into a dual-channel signal analyzer which retained the data in memory. Subsequent to the completion of data acquisition, a computer with access to this memory was used to determine statistically the mean velocities and their variances.

The flow was seeded by introducing 0.35- to 0.55-μm-diam polystyrene spheres into the settling chamber of the facility upstream of the model. This was necessary because of a lack of naturally occurring particles in the air supply system. An analysis of the response of the seed spheres to a normal shock wave indicated that a 99% velocity adjustment would occur in a distance of about 1 mm. A counting rate of a few thousand particles per second was obtained in the free stream.

These data were not corrected to account for the effects of velocity bias caused by particle averaging; such effects are believed to be small because of the fixed inactive time of the processors during pulse-stretching and other logic functions. This is conducive to a near-random sampling of measured velocities. Experiments were conducted to test this premise by electronically inhibiting the processors with a pseudorandom function generator set to various time scales. No significant effect was observed during these tests in the turbulent boundary-layer and wake regions. The excellent agreement in mean velocity from LDV and pitot-static measurements shown in figure 3 is also consistent with this result.

Flow Visualization

Conventional Schlieren and shadowgraph techniques were used for flow visualization. Surface flow on the flap was examined with an oil-flow technique using a mixture of titanium dioxide, oleic acid, and vacuum pump oil.

Accuracy of Measured Data

For the LDV measurements, three main sources of error were considered: optical, statistical, and positional. The optical errors include uncertainties in the measurement of beam angle and in alignment of the laser beams relative to the tunnel coordinate system. The statistical errors arise from the finite sample size. Typically, at least 5,000 samples were acquired at each measurement station. The errors introduced by each of the above sources were added to get an estimate of a probable maximum uncertainty. In practice, however, some of the errors could be compensating.

Quantity	Error
u/u_o	$\lesssim \pm 4\%$
k/u_o^2	$\lesssim \pm 8\%$
$\tau/(\rho u^2)_o$	$\lesssim \pm 8\%$
x	$\lesssim \pm 0.04$ cm
y	$\lesssim \pm 0.025$ cm

The mean velocity data determined from pitot-static measurements are estimated to be accurate to ±3%. Figure 3 shows good agreement between velocity profiles obtained from LDV and pitot-static measurements; the small differences are within the accuracy estimate stated above.

Two-Dimensionality of the Flow Field

Two dimensionality of the flow was evaluated from the following observations: (1) spanwise measurements of static pressure on the flat plate and flap over the central 20 cm of span, which showed negligible variation about centerline values; (2) surface-flow visualization, using the oil-flow technique, which showed surface streamlines nearly parallel to the main-stream direction over 90% of the span; and (3) estimates of the two-dimensional boundary-layer momentum balance. Results from these calculations are described next.

Symmetric flows- For the boundary layer (on the flap), the left-hand side (LHS) and right-hand side (RHS) of the integrated momentum equations are (ref. 10)

$$\text{LHS} = \frac{(\rho_e u_e^2 \theta)_x}{(\rho_e u_e^2 \theta)_{x_o}} - 1$$

$$\text{RHS} = \int_{x_o}^{x} \frac{\delta^* \, dp}{(\rho_e u_e^2 \theta)_{x_o}} + \int_{x_o}^{x} \frac{c_f}{2} \frac{\rho_e u_e^2}{(\rho_e u_e^2 \theta)_{x_o}} \, dx$$

For the wake, the above expressions hold, with the skin-friction term being zero.

The results of boundary-layer and wake momentum balances at $M_n = 0.4$ and 0.7 are shown in figures 4 and 5, respectively. In figures 4(a) and 5(a), x_o corresponds to the first measurement station on the flap ($x = -2.5$ cm). As may be seen, differences between the left-hand and right-hand sides arise in the vicinity of the trailing edge, and they remain downstream in the wake. These differences arise mainly because of the difficulty in estimating the pressure-gradient contribution close to the trailing edge. This view is supported by the results shown in figures 4(b) and 5(b) in which only the wake momentum balance is considered. In figures 4(b) and 5(b), x_o corresponds to the first measurement station in the wake ($x_o = 0.08$ cm). The vertical bars in figures 4 and 5 indicate the sensitivity of the results owing to a ±5% uncertainty in the momentum thickness, which is typical in the measured data. The agreement between the left-hand and right-hand sides of the momentum equations is

very good except at the last measurement station in the wake at $M_n = 0.4$, where some difference is seen.

Asymmetric flow- For the boundary layer ahead of the trailing edge, the left and right sides of the integrated-momentum equations are identical to those described above for the symmetrical flows.

For the asymmetric wake formed downstream of the trailing edge, it is necessary to determine the momentum balance considering the wake as a whole, since there is interaction between the upper and lower sides of the wake. An approximate momentum integral equation, derived within the boundary-layer approximations (see the appendix for details) is used here.

The momentum-balance results are shown in figure 6. For the boundary layers on the flap, x_o corresponds to the first measurement station on the flap ($x_o = -2.5$ cm). Good agreement between the left-hand and right-hand sides may be seen. For reasons described earlier, the results for the wake alone are shown in figure 6(b), and x_o corresponds to the first measurement station in the wake ($x_o = 0.15$ cm). The left and right sides again represent terms similar to those mentioned above for the boundary layer, with the skin-friction term being zero (see appendix). The measured static pressure data on $y = 0$ are used to evaluate the right-hand side of the momentum equations. The vertical bar indicates the sensitivity of the results that could arise from a ±5% uncertainty in the value of the integral I (see appendix) which is typical in the measured data. There is excellent agreement between the left and right sides in the wake.

Based on all these different observations and momentum balance estimates, mean flow two-dimensionality for all three cases is considered very good.

EXPERIMENTAL RESULTS

Symmetrical Trailing-Edge Flows

Symmetrical trailing-edge flows were obtained with zero flap deflection ($\alpha = 0°$) at nominal Mach numbers of 0.4 and 0.7.

Surface quantities- Model static-pressure distributions, normalized by the tunnel total pressure P_T, are shown in figure 7 for $M_n = 0.4$ and 0.7. The wake centerline pressures, as measured by the static-pressure probes, are also shown. Because of the excellent symmetry observed in the model pressure distribution, only the upper-surface pressures are shown in figure 7. The pressures on the flat plate are nearly constant, but at different levels for each M_n. The sudden decrease in the surface pressures at the junction of the flat plate and flap is a result of the rapid change in surface curvature. The flows do not involve shocks and the Mach number has only reached sonic value ($p/P_T = 0.528$, fig. 7) locally at the flap hinge line. The magnitudes of adverse pressure gradients on the flap increase with Mach number. There is a weak favorable pressure gradient in the near-wake region.

Model and tunnel-wall static-pressure distributions at $M_n = 0.4$ and 0.7 are presented in tables 1 and 2, respectively.

The skin-friction measurements at both Mach numbers, obtained with the hot-wire gauges, are displayed in figure 8. Measurements for only the upper surface of the

flap are shown because of the symmetrical nature of the flow. The decreasing trend of c_f along the flap caused by adverse pressure gradients is evident at $M_n = 0.7$. The vertical bars in figure 8 indicate estimated uncertainty in the skin-friction data. The c_f values obtained by fitting the measured velocity data to the law-of-the-wall are also shown.

Flow visualization- Spark shadowgraphs of the trailing-edge flow fields at $M_n = 0.4$ and 0.7 are shown in figure 9. The turbulent flow in the shear layers upstream and downstream of the trailing edge can be discerned from the outer flow.

Mean flow field- The measured mean-velocity profiles on the flat plate at a station 20.4 cm upstream of the trailing edge are shown in figure 10 in law-of-the-wall coordinates at both free-stream Mach numbers. Good agreement with the law-of-the-wall indicates a fully developed, turbulent boundary layer upstream of the flap. The mean-velocity data along with boundary-layer integral-thickness parameters are listed in tables 3 and 4.

All the experimental data that follow are presented in a suitably nondimensionalized form; the normalizing values are given in table 5. For the symmetrical flow, conditions at the edge of the boundary layer close to the trailing edge ($x = -0.4$ cm) at each Mach number are chosen for normalization. For the asymmetrical case, the data are normalized by boundary-layer-edge conditions on the flat-plate upper surface ($x = -30$ cm).

A typical example of flow symmetry is shown in figure 11. Mean-velocity and turbulent shear-stress profiles, as measured by the LDV, are shown for the symmetrical case at one streamwise position in the near-wake. The mean-velocity profile is symmetrical to within ±3%. A small asymmetry was observed in the position of the wake centerline at both values of M_n (0.4, 0.7); it did not coincide with the model centerline, but was progressively displaced downward. For example, this displacement at $M_n = 0.7$ was about 0.15 cm ($\delta_o/10$) at the farthest downstream x-station ($x = 14$ cm). We believe this asymmetry is due to the tunnel flow characteristics rather than model asymmetry. All velocity profiles were symmetric about the wake centerline to the same degree mentioned above. In view of the reasonably good symmetry observed about the wake centerline, most of the LDV measurements were limited to the lower half of the wake. However, most pitot- and static-pressure profiles were measured on both sides of the wake. In the figures and tables to follow, data will be presented for only one half of the wake.

Mean-velocity profiles in the trailing-edge and near-wake regions at $M_n = 0.7$ are shown in figure 12. As may be seen, measurements were made at stations quite close to the trailing edge. The y-values are corrected for the slight displacement of the wake centerline discussed earlier. The negative and positive values of the x/θ_o correspond to streamwise stations upstream and downstream of the trailing edge, respectively. Qualitatively similar results were seen at $M_n = 0.4$.

The mean-velocity data at $M_n = 0.4$ and 0.7 are presented in tables 6 and 7, respectively. These velocity data are those obtained from the pitot-static surveys rather than from the LDV. The pitot-static data are used because a larger number of more closely spaced y-positions were covered at each x-station during the pitot-static measurements.

Static-pressure profiles measured in the near-wake are displayed in figure 13 at both Mach numbers. The conical-nose probe was used at the first station downstream of the trailing edge and the elipsoidal-nose probe was used at the other downstream

stations. The probes were used with axes parallel to the x-axis. The probe data have not been corrected for flow-inclination effects; these corrections may be important in a small region around $y = 0$ at x-stations close to the trailing edge. The probes used had two static holes (180° apart) to minimize flow-incidence corrections.

The boundary-layer and wake integral-thickness parameters for both Mach numbers are given in table 8.

Turbulence flow field- Streamwise variations of turbulent shear-stress (τ_t) and kinetic-energy (k) profiles at $M_n = 0.7$ are shown in figures 14 and 15, respectively. The density information required for obtaining $\tau_t (= -\bar{\rho}\overline{u'v'})$ was determined from measurements of pitot and static pressures. To obtain the total values of k, the contribution from $\langle w'^2 \rangle$ was assumed equal to $1/2[\langle u'^2 \rangle + \langle v'^2 \rangle]$. Qualitatively similar results were observed at $M_n = 0.4$.

Data of turbulent shear-stress and kinetic-energy profiles at both Mach numbers are given in tables 6 and 7.

Asymmetric Trailing-Edge Flow

Asymmetric trailing-edge flow was obtained with a downward flap deflection of 6.25° at a nominal Mach number of 0.4.

Surface quantities- Figure 16 shows the model static-pressure distributions normalized by P_T. As may be seen, circulation is developed around the model, and the static pressures on the upper and lower surfaces of the flat plate are practically constant, although at different levels; the corresponding Mach numbers are 0.48 (upper surface) and 0.39 (lower surface). On the upper surface, the flow accelerates toward the hinge line and decelerates on the flap. Model and tunnel-wall static pressures are presented in tables 9 and 10, respectively.

Mean-velocity measurements of the boundary layer were not made on the upper surface of the flat-plate forebody. However, wall shear-stress measurements were made at $x/L = -0.220$, using a Preston tube; c_f had a value of 0.0022 at this station.

Skin-friction measurements on the upper and lower surfaces of the flap are shown in figure 17. A decreasing trend in c_f toward the trailing edge on the upper surface, caused by adverse pressure gradients, may be seen. The vertical bar in the figure represents an estimate of typical uncertainty in the data.

Flow visualization- A spark shadowgraph of the asymmetric trailing-edge flow field is shown in figure 18. The turbulent flow in the boundary layers and in the wake may be seen.

Mean flow field- Mean-velocity profiles in the trailing-edge and near-wake regions, measured with the LDV, are shown in figure 19. Data for both sides of the flow are shown. In this figure, as well as in subsequent ones, lines are drawn through the data points for clarity. Again, the negative and positive values of x correspond to measurement stations upstream and downstream of the trailing edge, respectively. Upstream of the trailing edge, the profiles on the upper surface are thicker and less full compared to those on the lower surface, reflecting the effects of adverse pressure gradients. The mean-velocity data shown in figure 19 are presented in table 11.

Near-wake static-pressure profiles, measured with the static pressure probes, are shown in figure 20. The conical-nose probe was used at $x = 0.15$ cm and the ellipsoidal-nose probe was used at downstream stations. The probes were used in a manner similar to that already described for the symmetric flows.

The boundary-layer and wake displacement-thickness distributions are listed in table 12. In the wake, as an approximation, the flow was divided into two parts about the minimum-velocity line, and the integral-thickness parameters were estimated independently for the upper and lower flows.

Turbulence flow field- The streamwise development of the turbulent shear-stress and kinetic-energy profiles is shown in figures 21 and 22, respectively. The manner in which τ_t and k are obtained has been described with regard to the symmetrical flows. Large, normal gradients in the vicinity of the minimum-velocity location are seen in the shear-stress profiles. Both the shear-stress and kinetic-energy profiles exhibit two peaks corresponding to the upper and lower sides of the near-wake. These data are presented in table 11.

CONCLUDING REMARKS

Experimental data for two-dimensional, trailing-edge flows at high Reynolds numbers are presented. Both symmetrical and asymmetrical flows, with pressure gradients upstream of the trailing edge, were investigated. The measurements made are of sufficient detail and quality for use in assessing turbulence models and prediction methods.

Since the experiment was carried out in a wind-tunnel test section that has solid upper and lower walls, wall effects may be important, particularly at the high Mach numbers. Any calculation method used in attempts to predict the entire flow field should include the effects of tunnel walls. Measured tunnel-wall static pressures may be used as boundary conditions or for verifying any modeling of the tunnel walls that may be employed in the prediction method.

APPENDIX

APPROXIMATE MOMENTUM INTEGRAL EQUATION FOR AN ASYMMETRIC WAKE

The flow under consideration has two different edge velocities (see fig. 23), which are caused by static-pressure variations normal to the flow direction. Also, there is interaction between the upper and lower sides of the wake. In deriving the momentum integral equation, therefore, it is necessary to treat the upper and lower sides of the wake together.

For the control volume shown (fig. 23), equating the net outgoing momentum flux to the net forces, we get

$$\frac{\partial}{\partial x}\int_0^h \rho u^2\, dy - M^* = -h\,\frac{dp}{dx} \tag{A1}$$

(Shear stresses are zero at the edges of the control volume.)

In equation (A1), M^* represents the total momentum flux (due to u_u and u_ℓ) entering the control volume just outside the wake from both sides. Since in general, $u_u \neq u_\ell$, it is difficult to estimate the individual contributions from upper and lower sides to obtain M^*. As an approximation, M^* is obtained using an average edge velocity:

$$u^* = \frac{1}{2}\,(u_u + u_\ell)$$

Therefore,

$$M^* = u^*\,\frac{\partial}{\partial x}\int_0^h \rho u\, dy$$

Equation (A1) can now be written as

$$\frac{\partial}{\partial x}\int_0^h \rho u^2\, dy - u^*\,\frac{\partial}{\partial x}\int_0^h \rho u\, dy = -h\,\frac{dp}{dx} \tag{A2}$$

The above approximation is likely to be satisfactory for relatively small differences between u_u and u_ℓ. For the asymmetrical wake described earlier, u_u and u_ℓ differ by about 4% in the vicinity of the trailing edge. The edge velocities are essentially the same at the last measurement station ($x = 14$ cm).

Integrating equation (A2) with respect to x from x_o to x and treating ρ as a constant (for simplicity), we get

$$\rho \int_{x_o}^{x} \left[\frac{\partial}{\partial x} \int_{o}^{h} \rho u^2 \, dy \right] dx - \rho \int_{x_o}^{x} \left[u^* \frac{\partial}{\partial x} \int_{o}^{h} \rho u \, dy \right] dx = - \int_{x_o}^{x} h \frac{dp}{dx} \, dx \qquad \text{(A3)}$$

we now define

$$\int_{o}^{h} u^2 \, dy = I \qquad \text{and} \qquad \int_{o}^{h} u \, dy = J$$

Inserting the above definitions into equation (A3), and after carrying out the integration and normalization by $I(x_o)$, the two sides of the momentum integral equation can be written as follows:

$$\text{LHS} = \frac{I(x)}{I(x_o)} - 1 - \frac{1}{I(x_o)} \int_{x_o}^{x} u^* \frac{\partial J}{\partial x} \, dx$$

$$\text{RHS} = - \frac{1}{\rho I(x_o)} \int_{x_o}^{x} h \frac{dp}{dx} \, dx$$

REFERENCES

1. Melnik, R. E.; Chow, R.; and Mead, H. R.: Theory of Viscous Transonic Flow Over Airfoils at High Reynolds Number. AIAA Paper 77-680, 1977.

2. Lock, R. C.: A Review of Methods for Predicting Viscous Effects on Aerofoils and Wings at Transonic Speeds. AGARD-CP-291, Feb. 1981.

3. Kline, S. J.; Cantwell, B. J.; and Liley, G. M., eds.: 1980-1981 AFOSR-HTTM-Stanford Conference on Complex Turbulent Flows: Comparisons of Computation and Experiments. Vol. I, Stanford University, Stanford, Calif., 1981.

4. Viswanath, P. R.; Cleary, J. W.; Seegmiller, H. L.; and Horstman, C. C.: Trailing-Edge Flows at High Reynolds Number. AIAA Paper 79-1503, 1979 (also AIAA J., vol. 18, Sept. 1980, pp. 1059-1065).

5. Cleary, J. W.; Viswanath, P. R.; Horstman, C. C.; and Seegmiller, H. L.: Asymmetric Trailing-Edge Flows at High Reynolds Number. AIAA Paper 80-1396, 1980.

6. Rubesin, M. W.; Okuno, A. F.; and Mateer, G. G.: A Hot-Wire Surface Gage for Skin Friction and Separation Detection Measurements. NASA TM X-62,465, 1975.

7. Murthy, V. S.; and Rose, W. C.: Direct Measurements of Wall Shear-Stress by Buried Wire Gages in a Shock Wave Boundary Layer Interaction Region. AIAA Paper 77-691, Albuquerque, N. Mex., 1977.

8. Wilcox, D. C.; and Rubesin, M. W.: Progress in Turbulence Modeling for Complex Flow Fields, Including Effects of Compressibility. NASA TP-1517, 1980.

9. Mateer, G. G.; and Viegas, J. R.: Effects of Mach and Reynolds Numbers on a Normal Shock-Wave/Turbulent-Boundary-Layer Interaction. AIAA Paper 79-1502, Williamsburg, Va., July 1979.

10. Alber, I. E.; Bacon, J. W.; Masson, B. S.; and Collins, D. J.: An Experimental Investigation of Turbulent Transonic Viscous-Inviscid Interactions. AIAA Paper 71-565, June 1971.

TABLE 1.- MODEL STATIC-PRESSURE DISTRIBUTIONS

$M_n = 0.4$, $Re_L = 24.3\times10^6$, $\alpha = 0°$		$M_n = 0.7$, $Re_L = 36.6\times10^6$, $\alpha = 0°$	
x/L	p/P_T	x/L	p/P_T
-.940	.888	-.940	.698
-.973	.886	-.973	.689
-.809	.883	-.809	.674
-.775	.880	-.775	.663
-.742	.872	-.742	.635
-.704	.877	-.704	.646
-.672	.878	-.672	.648
-.607	.878	-.607	.648
-.541	.880	-.541	.650
-.475	.878	-.475	.644
-.409	.879	-.409	.643
-.344	.878	-.344	.640
-.278	.877	-.278	.637
-.213	.876	-.213	.632
-.180	.874	-.180	.625
-.146	.867	-.146	.605
-.124	.843	-.124	.510
-.117	.861	-.117	.581
-.103	.870	-.103	.622
-.094	.874	-.094	.642
-.083	.878	-.083	.652
-.073	.881	-.073	.663
-.064	.884	-.064	.674
-.052	.886	-.052	.682
-.042	.891	-.042	.690
-.032	.892	-.032	.698
-.024	.895	-.024	.709
-.022	.896	-.022	.710
-.013	.897	-.013	.714
-.005	.903	-.005	.728
.008	.902	.008	.722
.025	.899	.025	.717
.150	.892	.150	.698

Note: For $x/L > 0$, static pressure values on $y = 0$ are presented.

TABLE 2.- TUNNEL-WALL STATIC-PRESSURE DISTRIBUTIONS

$M_n = 0.4$, $Re_L = 24.3\times10^6$, $\alpha = 0°$		$M_n = 0.7$, $Re_L = 36.6\times10^6$, $\alpha = 0°$	
x/L	p/P_T	x/L	p/P_T
-1.027	.895	-1.027	.724
-.918	.892	-.918	.712
-.809	.884	-.809	.685
-.700	.882	-.700	.663
-.591	.880	-.591	.651
-.482	.878	-.482	.644
-.373	.878	-.373	.642
-.264	.877	-.264	.636
-.155	.878	-.155	.637
-.046	.882	-.046	.659
.063	.888	.063	.693
.172	.889	.172	.698
.281	.896	.281	.701
.390	.892	.390	.699
.499	.893	.499	.702
.608	.894	.608	.710

TABLE 3.- FLAT-PLATE BOUNDARY-LAYER PROFILE

$x/L = 0.220$, $M_n = 0.4$, $Re_L = 24.3\times10^6$, $\alpha = 0°$			
y, cm	u/u_o	y, cm	u/u_o
0.000	0.000	.157	.905
.013	.590	.170	.913
.023	.650	.191	.922
.033	.742	.221	.938
.043	.783	.267	.965
.053	.795	.368	1.010
.063	.815	.495	1.053
.076	.828	.584	1.076
.089	.846	.686	1.098
.099	.856	.744	1.106
.109	.868	.795	1.115
.119	.876	.851	1.122
.129	.882	.902	1.128
.140	.888	1.000	1.136

Note: Displacement thickness = 0.110 cm;
momentum thickness = 0.083 cm.

TABLE 4.- FLAT-PLATE BOUNDARY-LAYER PROFILE

$x/L = 0.220$, $M_n = 0.7$, $Re_L = 36.6\times10^6$, $\alpha = 0°$			
y, cm	u/u_o	y, cm	u/u_o
0.000	0.000	.213	.981
.013	.613	.292	1.010
.023	.675	.394	1.048
.033	.738	.445	1.066
.043	.773	.551	1.096
.053	.807	.660	1.124
.066	.833	.762	1.146
.076	.854	.864	1.164
.086	.876	.927	1.171
.109	.897	1.029	1.179
.129	.918	1.130	1.184
.160	.940	1.183	1.188
.191	.963		

Note: Displacement thickness = 0.140 cm;
momentum thickness = 0.089 cm.

TABLE 5.- REFERENCE VALUES FOR NORMALIZING DATA

M_n	u_o, m/sec	$(\rho u_o^2)_o$, N/m^2	α, deg	δ_o^*, cm	θ_o, cm
0.4	124.2	5.163×10^4	0	0.230	0.147
.7	215.8	1.337×10^5	0	.363	.195
.4	153.6	7.592×10^4	6.25		

TABLE 6.- BOUNDARY-LAYER AND WAKE PROFILES: MEAN AND TURBULENCE DATA

$M_n = 0.4$, $Re_L = 24.3 \times 10^6$, $\alpha = 0°$

y, cm	u/u_o	y, cm	k/u_o^2	$\tau_t/(\rho u^2)_o$
		$x/\theta_o = -17.2$		
0.000	0.	0.000	0.	0.
.013	4.90E-01	.180	7.70E-03	1.91E-03
.023	5.20E-01	.230	6.96E-03	1.59E-03
.033	5.52E-01	.281	7.21E-03	1.75E-03
.043	5.90E-01	.331	5.86E-03	1.31E-03
.056	6.10E-01	.382	5.61E-03	1.19E-03
.066	6.24E-01	.484	4.26E-03	8.10E-04
.076	6.40E-01	.611	3.94E-03	7.60E-04
.086	6.53E-01	.740	3.60E-03	6.60E-04
.097	6.70E-01	.992	2.78E-03	6.90E-04
.107	6.80E-01	1.250	1.76E-03	2.10E-04
.117	6.92E-01	1.750	1.36E-03	2.20E-04
.129	7.00E-01			
.150	7.14E-01			
.191	7.40E-01			
.254	7.83E-01			
.356	8.40E-01			
.419	8.70E-01			
.483	8.94E-01			
.584	9.30E-01			
.686	9.64E-01			
.795	9.94E-01			
.902	1.02E+00			
1.000	1.03E+00			
1.110	1.04E+00			
1.160	1.05E+00			
		$x/\theta_o = -2.7$		
0.000	0.	0.000	0.	0.
.035	5.10E-01	.134	7.68E-03	1.77E-03
.046	5.20E-01	.185	7.47E-03	1.94E-03
.056	5.30E-01	.236	7.40E-03	1.96E-03
.066	5.41E-01	.286	6.78E-03	1.93E-03
.079	5.54E-01	.337	7.09E-03	2.01E-03
.091	5.63E-01	.464	5.07E-03	1.42E-03
.101	5.72E-01	.591	4.62E-03	1.19E-03
.109	5.80E-01	.720	3.82E-03	8.30E-04
.119	5.86E-01	.972	2.44E-03	5.90E-04
.129	5.92E-01	1.230	1.43E-03	2.40E-04
.152	6.18E-01	1.734	1.06E-03	1.00E-05
.175	6.42E-01	1.990	1.18E-03	0.
.236	6.90E-01			
.310	7.40E-01			
.411	7.80E-01			
.570	8.50E-01			
.680	8.90E-01			
.840	9.30E-01			
1.050	9.64E-01			
1.260	9.90E-01			
1.360	1.00E+00			

TABLE 6.- CONTINUED

$M_n = 0.4$, $Re_L = 24.3\times10^6$, $\alpha = 0°$				
y, cm	u/u_o	y, cm	k/u_o^2	$\tau_t/(\rho u^2)_o$
		$x/\theta_o = 0.8$		
0.000	4.00E-01	0.000		0.
.038	4.53E-01	.075	7.82E-03	2.10E-03
.063	5.00E-01	.152	8.26E-03	1.81E-03
.152	5.90E-01	.280	7.44E-03	1.93E-03
.254	6.50E-01	.406	7.48E-03	1.91E-03
.355	7.20E-01	.533	5.44E-03	1.40E-03
.470	7.70E-01	.787	3.40E-03	6.60E-04
.596	8.20E-01	1.041	2.14E-03	3.80E-04
.700	8.50E-01	1.295	1.02E-03	1.00E-04
.800	8.76E-01	1.550	7.80E-04	-4.00E-05
.900	9.00E-01	2.050	7.30E-04	-5.00E-05
1.110	9.43E-01			
1.330	9.70E-01			
1.540	9.90E-01			
1.580	9.93E-01			
		$x/\theta_o = 4.3$		
0.000	4.80E-01	0.000	6.46E-03	0.
.025	5.20E-01	.051	6.95E-03	1.21E-03
.127	5.90E-01	.127	8.80E-03	2.76E-03
.228	6.70E-01	.254	8.36E-03	2.70E-03
.343	7.31E-01	.381	7.44E-03	2.48E-03
.444	7.80E-01	.510	6.61E-03	1.88E-03
.546	8.23E-01	.762	4.47E-03	1.24E-03
.610	8.44E-01	1.020	3.50E-03	8.30E-04
.711	8.70E-01	1.270	2.14E-03	4.40E-04
.826	9.10E-01	1.524	1.51E-03	3.10E-04
.927	9.30E-01	2.030	1.12E-03	2.10E-04
1.030	9.50E-01			
1.143	9.61E-01			
1.346	9.86E-01			
1.626	1.00E+00			
		$x/\theta_o = 15.2$		
0.000	6.20E-01	0.000	5.98E-03	0.
.025	6.40E-01	.076	5.88E-03	1.03E-03
.076	6.51E-01	.203	7.58E-03	2.35E-03
.127	6.70E-01	.254	8.02E-03	2.64E-03
.191	6.90E-01	.330	7.78E-03	2.48E-03
.292	7.40E-01	.460	6.90E-03	2.12E-03
.394	7.80E-01	.584	5.98E-03	1.77E-03
.510	8.25E-01	.711	4.52E-03	1.21E-03
.610	8.60E-01	.965	3.38E-03	8.20E-04
.710	8.90E-01	1.473	1.41E-03	3.90E-04
.826	9.25E-01	1.980	1.02E-03	2.70E-04
.927	9.43E-01			
1.030	9.70E-01			
1.140	9.91E-01			
1.240	1.01E+00			
1.350	1.02E+00			
1.460	1.02E+00			
1.650	1.03E+00			

TABLE 6.- CONCLUDED

$M_n = 0.4$, $Re_L = 24.3\times10^6$, $\alpha = 0°$				
y, cm	u/u_o	y, cm	k/u_o^2	$\tau_t/(\rho u^2)_o$
$x/\theta_o = 43.0$				
0.000	.722		4.37E-03	0.
.127	.732		5.05E-03	9.40E-04
.254	.760		6.32E-03	1.51E-03
.381	.800		6.20E-03	1.70E-03
.635	.893		5.01E-03	1.15E-03
.890	.950		3.26E-03	6.10E-04
1.400	1.022		1.26E-03	1.50E-04
1.651	1.030		9.70E-04	6.00E-05
1.905	1.040		6.80E-04	4.00E-05
$x/\theta_o = 60.1$[a]				
0.000	.740			
.101	.750			
.216	.760			
.318	.790			
.419	.812			
.521	.850			
.635	.883			
.737	.905			
.864	.940			
1.070	.974			
1.270	1.010			
1.470	1.023			
1.670	1.036			
$x/\theta_o = 94.5$				
0.000	8.00E-01	0.000	4.37E-03	0.
.114	8.00E-01	.101	5.10E-03	1.60E-04
.203	8.10E-01	.230	4.47E-03	8.60E-04
.305	8.30E-01	.355	5.01E-03	1.32E-03
.406	8.46E-01	.610	5.98E-03	1.66E-03
.533	8.73E-01	.863	5.93E-03	1.58E-03
.635	9.06E-01	1.370	2.43E-03	7.80E-04
.737	9.33E-01	1.880	9.20E-04	3.30E-04
.840	9.50E-01	2.390	8.30E-04	3.00E-04
.940	9.64E-01			
1.040	9.90E-01			
1.240	1.00E+00			
1.470	1.00E+00			

[a]Turbulence measurements were not made at this station.

TABLE 7.- BOUNDARY-LAYER AND WAKE PROFILES: MEAN AND TURBULENCE DATA

$M_n = 0.7$, $Re_L = 36.6 \times 10^6$, $\alpha = 0°$

y, cm	u/u_o	y, cm	k/u_o^2	$\tau_t/(\rho u^2)_o$
		$x/\theta_o = -13.0$		
0.000	0.	0.000	0.	0.
.013	3.91E-01	.230	9.29E-03	2.43E-03
.025	4.23E-01	.280	9.50E-03	2.46E-03
.051	4.80E-01	.331	8.48E-03	2.31E-03
.064	5.00E-01	.382	7.90E-03	2.21E-03
.076	5.25E-01	.484	6.60E-03	1.75E-03
.089	5.40E-01	.737	3.75E-03	1.00E-03
.102	5.60E-01	.992	2.90E-03	6.90E-04
.114	5.70E-01	1.500	1.44E-03	2.10E-04
.140	5.92E-01	2.000	1.30E-03	1.00E-04
.191	6.40E-01			
.216	6.80E-01			
.267	6.95E-01			
.318	7.30E-01			
.368	7.60E-01			
.470	8.20E-01			
.635	8.83E-01			
.851	9.50E-01			
1.100	1.01E+00			
1.470	1.04E+00			
		$x/\theta_o = -2.0$		
0.000	0.	0.000	0.	0.
.038	3.80E-01	.134	1.05E-02	2.65E-03
.050	4.00E-01	.185	1.04E-02	2.87E-03
.064	4.22E-01	.235	1.08E-02	3.04E-03
.089	4.56E-01	.286	1.07E-02	3.07E-03
.102	4.74E-01	.340	1.18E-02	3.19E-03
.127	5.00E-01	.464	8.37E-03	2.47E-03
.165	5.20E-01	.592	7.65E-03	2.15E-03
.178	5.40E-01	.720	5.33E-03	1.53E-03
.228	5.70E-01	.972	3.65E-03	1.07E-03
.280	5.94E-01	1.480	1.58E-03	3.60E-04
.330	6.30E-01	1.990	1.24E-03	1.90E-04
.380	6.50E-01	2.490	1.27E-03	1.50E-04
.430	6.70E-01			
.533	7.30E-01			
.635	7.80E-01			
.736	8.18E-01			
.863	8.70E-01			
1.070	9.24E-01			
1.270	9.70E-01			
1.470	9.92E-01			
1.600	1.00E+00			

TABLE 7.- CONTINUED

$M_n = 0.7$, $Re_L = 36.6\times10^6$, $\alpha = 0°$				
y, cm	u/u_o	y, cm	k/u_o^2	$\tau_t/(\rho u^2)_o$
		$x/\theta_o = 0.6$		
0.000	3.20E-01	0.000	7.20E-03	0.
.043	4.00E-01	.038	9.11E-03	2.81E-03
.076	4.40E-01	.114	9.95E-03	3.02E-03
.127	4.83E-01	.165	9.56E-03	2.98E-03
.165	5.10E-01	.216	1.03E-02	3.42E-03
.254	5.75E-01	.292	1.04E-02	3.67E-03
.381	6.14E-01	.420	9.85E-03	3.54E-03
.482	7.06E-01	.550	8.55E-03	3.03E-03
.597	7.61E-01	.800	5.44E-03	1.88E-03
.698	8.00E-01	1.050	3.22E-03	1.27E-03
.800	8.37E-01	1.310	2.29E-03	7.40E-04
.900	8.71E-01	1.820	9.00E-04	1.70E-04
1.000	9.00E-01	2.320	1.05E-03	7.00E-05
1.105	9.20E-01			
1.320	9.60E-01			
1.520	9.90E-01			
1.780	1.00E+00			
1.850	1.00E+00			
		$x/\theta_o = 3.2$		
0.000	4.20E-01	0.000	6.68E-03	0.
.063	5.20E-01	.051	9.03E-03	3.04E-03
.178	5.70E-01	.102	9.85E-03	3.63E-03
.254	6.17E-01	.254	1.06E-02	3.80E-03
.355	6.60E-01	.510	8.97E-03	3.20E-03
.457	7.06E-01	.760	5.25E-03	1.80E-03
.571	7.54E-01	1.016	3.08E-03	1.16E-03
.673	8.00E-01	1.270	2.24E-03	6.50E-04
.774	8.50E-01	1.520	1.18E-03	3.20E-04
.876	8.82E-01	2.032	8.90E-04	9.00E-05
.990	9.15E-01			
1.090	9.40E-01			
1.190	9.55E-01			
1.410	9.80E-01			
1.625	1.00E+00			
1.830	1.01E+00			
2.032	1.02E+00			
		$x/\theta_o = 11.6$		
0.000	5.30E-01	0.000	6.44E-03	0.
.025	5.50E-01	.076	6.83E-03	7.60E-04
.140	6.06E-01	.203	9.37E-03	2.88E-03
.185	6.26E-01	.330	1.02E-02	3.15E-03
.292	6.65E-01	.457	9.40E-03	2.78E-03
.394	7.04E-01	.711	6.15E-03	1.68E-03
.495	7.60E-01	.965	4.03E-03	1.09E-03
.610	8.00E-01	1.220	2.11E-03	5.70E-04
.711	8.42E-01	1.473	1.35E-03	3.10E-04
.813	8.80E-01	1.980	6.10E-04	2.10E-04
.927	9.10E-01			
1.030	9.37E-01			
1.130	9.60E-01			
1.244	9.80E-01			
1.346	9.92E-01			
1.450	1.01E+00			
1.663	1.02E+00			
1.880	1.02E+00			

TABLE 7.- CONCLUDED

$M_n = 0.7$, $Re_L = 36.6\times10^6$, $\alpha = 0^c$				
y, cm	u/u_o	y, cm	k/u_o^2	$\tau_t/(\rho u^2)_o$
		$x/\theta_o = 32.5$		
0.000	.670		6.42E-03	0.
.101	.680		6.17E-03	1.06E-03
.228	.700		7.29E-03	1.97E-03
.356	.746		8.06E-03	2.44E-03
.610	.834		7.13E-03	1.93E-03
.863	.913		4.52E-03	1.23E-03
1.120	.970		2.62E-03	7.00E-04
1.372	1.005		1.47E-03	4.00E-04
1.880	1.040		6.50E-04	1.90E-04
2.380	1.040		3.50E-04	9.00E-05
		$x/\theta_o = 45.5^a$		
0.000	.690			
.051	.690			
.152	.700			
.280	.714			
.380	.742			
.483	.780			
.584	.812			
.696	.843			
.800	.874			
.902	.902			
1.000	.930			
1.117	.953			
1.220	.975			
1.320	.994			
1.540	1.013			
1.910	1.032			
2.090	1.040			
		$x/\theta_o = 71.4$		
0.000	7.70E-01	0.000	5.44E-03	0.
.114	7.70E-01	.025	5.47E-03	0.
.203	7.71E-01	.280	5.61E-03	1.16E-03
.305	7.83E-01	.533	7.53E-03	1.80E-03
.406	8.15E-01	.790	6.93E-03	1.81E-03
.495	8.30E-01	1.295	3.17E-03	7.50E-04
.622	8.60E-01	1.803	9.50E-04	2.60E-04
.724	8.81E-01	2.311	4.50E-04	1.50E-04
.826	9.00E-01			
.949	9.27E-01			
1.040	9.60E-01			
1.143	9.80E-01			
1.260	1.00E+00			
1.470	1.02E+00			
1.575	1.03E+00			
2.000	1.04E+00			
2.190	1.05E+00			

[a] Turbulence measurements were not made at this station.

TABLE 8.- BOUNDARY-LAYER AND WAKE MOMENTUM-INTEGRAL PARAMETERS

$M_n = 0.4$, $Re_L = 24.3\times10^6$, $\alpha = 0°$			$M_n = 0.7$, $Re_L = 36.6\times10^6$, $\alpha = 0°$		
x/θ_o	δ^*, cm	θ, cm	x/θ_o	δ^*, cm	θ, cm
-17.200	.180	.120	-13.000	.290	.160
-2.700	.230	.150	-2.000	.360	.200
.800	.270	.180	.600	.380	.210
4.300	.250	.170	3.250	.360	.210
15.200	.230	.160	11.600	.320	.200
60.000	.210	.160	45.500	.310	.200
94.500	.150	.130	71.400	.270	.180

TABLE 9.- MODEL STATIC-PRESSURE DISTRIBUTIONS

$M_n = 0.4$, $Re_L = 24.3\times10^6$, $\alpha = 6.25°$			
Upper surface		Lower surface	
x/L	p/P_T	x/L	p/P_T
-.940	.863	-.940	.910
-.973	.863	-.973	.907
-.809	.860	-.809	.903
-.775	.857	-.775	.902
-.742	.851	-.742	.898
-.704	.853	-.704	.899
-.672	.853	-.672	.899
-.607	.855	-.607	.899
-.541	.856	-.541	.900
-.475	.255	-.475	.900
-.409	.854	-.409	.899
-.344	.853	-.344	.900
-.278	.852	-.278	.898
-.213	.849	-.213	.897
-.180		-.180	.898
-.146	.823	-.146	.897
-.124	.774	-.124	.895
-.117	.816	-.117	.897
-.103	.840	-.103	.898
-.094	.851	-.083	.897
-.083	.858	-.064	.897
-.073	.865	-.042	.897
-.064	.870	-.005	.899
-.052	.876		
-.042			
-.032	.878		
-.024	.889		
-.022	.891		
-.013	.894		
-.005	.898		
.008	.901		
.025	.897		
.150	.892		

Note: For $x/L > 0$, static-pressure values on $y = 0$ are presented.

TABLE 10.- TUNNEL-WALL STATIC-PRESSURE DISTRIBUTIONS

$M_n = 0.4$, $Re_L = 24.3\times10^6$, $\alpha = 6.25°$		
x/L	Upper wall	Lower wall
	p/P_T	p/P_T
-1.027	.882	.909
-.918	.875	
-.809	.865	.885
-.700	.859	.906
-.591	.856	.909
-.482	.854	.907
-.373	.853	.906
-.264	.853	.903
-.155	.856	.903
-.046	.864	.898
.063	.879	.897
.172	.884	.895
.281	.893	.893
.390	.891	.891
.499	.891	.890
.608	.893	.894

TABLE 11.- BOUNDARY-LAYER AND WAKE PROFILES: MEAN AND TURBULENCE DATA

$M_n = 0.4$, $Re_L = 24.3 \times 10^6$, $\alpha = 6.25°$

y, cm	u/u_o	k/u_o^2	$\tau_t/(\rho u^2)_o$
	x = -2.5 cm (upper surface)		
0.000	0.000	0.	0.
.147	.410	7.80E-03	2.69E-03
.200	.460	7.68E-03	2.71E-03
.250	.493	7.71E-03	2.63E-03
.300	.530	7.62E-03	2.65E-03
.400	.583	6.69E-03	2.25E-03
.503	.642	4.75E-03	1.47E-03
.604	.690	3.65E-03	1.10E-03
.705	.722	2.96E-03	9.30E-04
1.987	.814	1.78E-03	4.60E-04
1.479	.860	9.10E-04	1.90E-04
1.976	.886	8.50E-04	1.10E-04
2.480	.900	9.90E-04	2.00E-05
	x = -0.4 cm (upper surface)		
0.000	0.000	0.	0.
.114	.300	7.33E-03	2.11E-03
.165	.330	7.17E-03	2.29E-03
.216	.351	8.32E-03	2.63E-03
.267	.370	8.10E-03	2.46E-03
.370	.430	8.48E-03	2.76E-03
.470	.494	7.87E-03	2.61E-03
.673	.605	6.08E-03	1.88E-03
.930	.705	3.21E-03	9.60E-04
1.181	.764	2.46E-03	6.80E-04
1.690	.840	9.50E-04	1.90E-04
2.197	.860	8.30E-04	1.40E-04
2.705	.870	9.10E-04	8.00E-05
	x = -2.5 cm (lower surface)		
0.000	0.000	0.	0.
-.152	.670	2.85E-03	-4.70E-04
-.203	.690	3.14E-03	-6.00E-04
-.254	.700	2.72E-03	-5.10E-04
-.305	.710	2.69E-03	-5.30E-04
-.355	.726	2.65E-03	-5.30E-04
-.406	.742	2.26E-03	-4.30E-04
-.510	.760	2.14E-03	-3.90E-04
-.635	.790	1.68E-03	-2.90E-04
-.760	.800	1.12E-03	-1.80E-04
-.890	.813	7.40E-04	-6.00E-05
-1.016	.820	5.10E-04	-1.00E-05
-1.270	.830	4.30E-04	4.00E-05

TABLE 11.- CONTINUED

$M_n = 0.4$, $Re_L = 24.3\times10^6$, $\alpha = 6.25°$			
y, cm	u/u_o	k/u_o^2	$\tau_t/(\rho u^2)_o$
x = -0.4 cm (lower surface)			
0.000	0.000	0.	0.
-.051	.600	3.97E-03	-5.50E-04
-.102	.644	3.68E-03	-5.30E-04
-.152	.664	3.40E-03	-5.90E-04
-.203	.690	3.01E-03	-5.10E-04
-.254	.700	2.85E-03	-5.50E-04
-.305	.711	2.46E-03	-4.90E-04
-.508	.755	2.30E-03	-4.90E-04
-.762	.800	1.25E-03	-1.90E-04
-1.016	.820	6.40E-04	-8.00E-05
-1.520	.826	3.30E-04	3.00E-05
x = 0.15 cm			
-1.245	.810	7.80E-04	-2.00E-04
-.991	.783	1.36E-03	-3.80E-04
-.737	.740	2.14E-03	-5.20E-04
-.483	.690	2.77E-03	-6.50E-04
-.102	.560	4.12E-03	-7.20E-04
-.025	.260	4.86E-03	-2.80E-03
.025	.211	5.42E-03	1.29E-03
.076	.244	6.40E-03	1.65E-03
.152	.304	8.15E-03	2.23E-03
.280	.360	8.38E-03	2.79E-03
.380	.420	8.74E-03	3.03E-03
.533	.501	9.60E-03	3.05E-03
.787	.635	5.31E-03	1.72E-03
1.041	.724	3.07E-03	8.80E-04
1.295	.782	1.81E-03	4.30E-04
1.803	.830	7.00E-04	1.10E-04
2.311	.845	6.40E-04	6.00E-05
2.820	.850	8.10E-04	0.
x = 0.7 cm			
-1.780	.810	4.90E-04	-1.00E-04
-1.270	.790	1.07E-03	-1.90E-04
-.762	.736	2.29E-03	-4.80E-04
-.510	.690	2.80E-03	-6.40E-04
-.254	.614	4.05E-03	-8.20E-04
-.130	.540	6.21E-03	-1.64E-03
-.051	.420	8.67E-03	-2.69E-03
0.000	.332	6.93E-03	-1.14E-03
.130	.334	7.53E-03	2.05E-03
.203	.370	9.38E-03	2.94E-03
.254	.396	8.86E-03	2.92E-03
.305	.404	8.64E-03	2.92E-03
.381	.452	8.75E-03	2.81E-03
.510	.523	8.41E-03	2.64E-03
.762	.644	5.20E-03	1.60E-03
1.020	.726	2.76E-03	7.60E-04
1.270	.780	1.80E-03	4.40E-04
1.524	.800	1.24E-03	2.80E-04
1.780	.815	8.60E-04	1.10E-04
2.032	.823	8.60E-04	1.70E-04
2.540	.840	1.00E-03	2.40E-04

TABLE 11.- CONTINUED

$M_n = 0.4$, $Re_L = 24.3\times10^6$, $\alpha = 6.25°$			
y, cm	u/u_o	k/u_o^2	$\tau_t/(\rho u^2)_o$
x = 2.3 cm			
-1.730	.820	4.50E-04	-9.00E-05
-1.220	.810	9.30E-04	-3.20E-04
-.711	.733	2.27E-03	-5.90E-04
-.460	.680	3.10E-03	-7.80E-04
-.330	.633	4.32E-03	-1.31E-03
-.203	.570	6.75E-03	-2.20E-03
-.127	.510	7.26E-03	-2.33E-03
-.076	.475	6.69E-03	-1.97E-03
.051	.430	5.92E-03	-1.10E-04
.178	.450	7.39E-03	1.93E-03
.305	.492	9.15E-03	2.88E-03
.432	.552	8.38E-03	2.78E-03
.560	.605	7.81E-03	2.61E-03
.690	.657	6.18E-03	2.03E-03
.813	.710	4.03E-03	1.36E-03
1.067	.770	2.40E-03	7.30E-04
1.321	.794	1.66E-03	5.10E-04
1.830	.840	8.30E-04	2.50E-04
2.340	.860	7.70E-04	2.30E-04
2.850	.870	9.80E-04	2.80E-04
x = 6.4 cm			
-1.651	.827	5.10E-04	2.00E-05
-1.143	.800	1.04E-03	-1.10E-04
-.635	.720	3.07E-03	-7.00E-04
-.381	.640	4.65E-03	-1.23E-03
-.127	.578	4.61E-03	-6.40E-04
0.000	.570	5.14E-03	6.10E-04
.127	.581	5.54E-03	1.62E-03
.254	.610	6.79E-03	2.31E-03
.381	.642	6.57E-03	2.35E-03
.510	.680	5.85E-03	2.14E-03
.635	.720	5.18E-03	1.86E-03
.890	.780	3.03E-03	1.25E-03
1.143	.813	1.41E-03	6.50E-04
1.400	.830	7.10E-04	3.00E-04
1.910	.846	4.90E-04	1.90E-04
2.413	.857	4.60E-04	1.80E-04
2.921	.870	5.40E-04	1.80E-04

TABLE 11.- CONCLUDED

$M_n = 0.4$, $Re_L = 24.3\times10^6$, $\alpha = 6.25°$			
y, cm	u/u_o	k/u_o^2	$\tau_t/(\rho u^2)_o$
x = 14 cm			
-2.134	.847	5.80E-04	-1.60E-04
-1.626	.834	9.80E-04	-2.60E-04
-1.118	.770	3.16E-03	-9.30E-04
-.864	.710	3.87E-03	-1.09E-03
-.610	.672	3.73E-03	-8.70E-04
-.360	.650	3.62E-03	-1.30E-04
-.230	.650	3.93E-03	3.40E-04
-.102	.670	5.19E-03	9.20E-04
.025	.663	4.33E-03	9.60E-04
.152	.696	6.09E-03	1.51E-03
.280	.712	5.23E-03	1.32E-03
.406	.755	6.10E-03	1.60E-03
.660	.780	4.17E-03	1.18E-03
.914	.830	2.44E-03	7.30E-04
1.170	.843	1.03E-03	1.70E-04
1.422	.850	1.02E-03	1.60E-04
1.930	.850	4.60E-04	-8.00E-05
2.440	.850	5.00E-04	-7.00E-05
2.950	.850	4.60E-04	-5.00E-05

TABLE 12.- BOUNDARY-LAYER AND WAKE DISPLACEMENT-THICKNESS DISTRIBUTIONS

$M_n = 0.4$, $Re_L = 24.3\times10^6$, $\alpha = 6.25°$		
x, cm	Upper	Lower
	δ^*, cm	δ^*, cm
-2.500	.380	.100
-.400	.500	.110
.150	.490	.200
.700	.420	.220
2.300	.380	.220
6.400	.280	.180
14.000	.180	.180

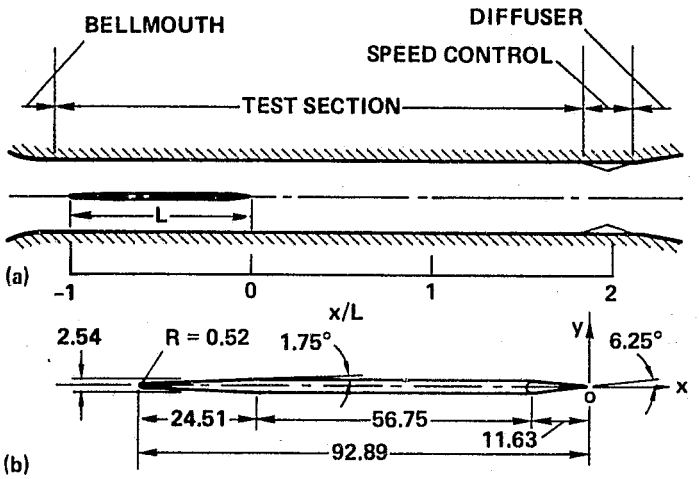

(a) Test section.

(b) Test model.

Figure 1.- Schematic of test section and test model.

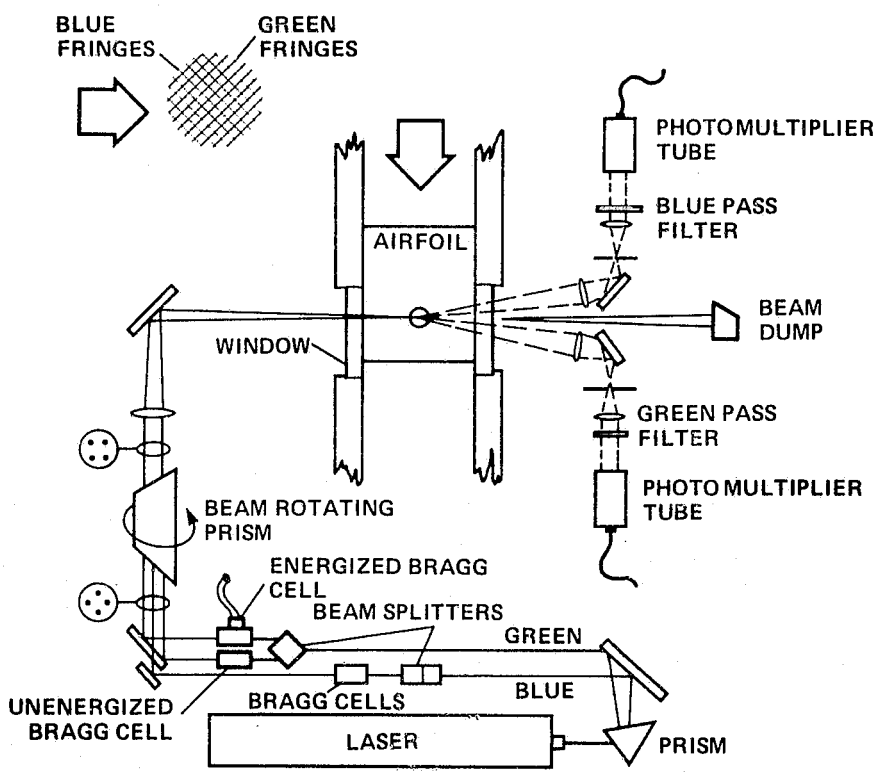

Figure 2.- Schematic of LDV optical arrangement.

ORIGINAL PAGE IS
OF POOR QUALITY

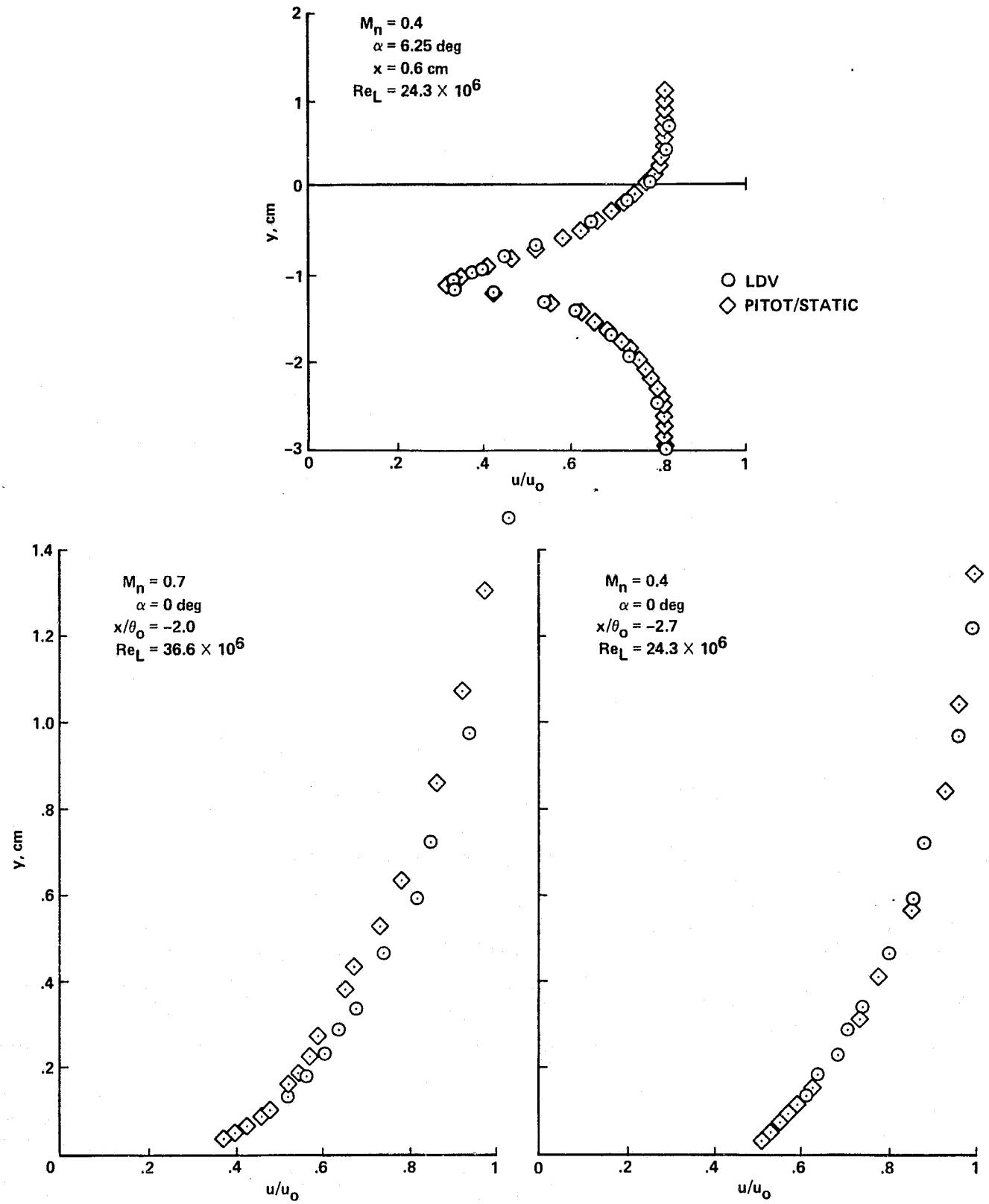

Figure 3.- Comparison of mean-velocity data from LDV and pitot-static measurements.

ORIGINAL PAGE IS
OF POOR QUALITY

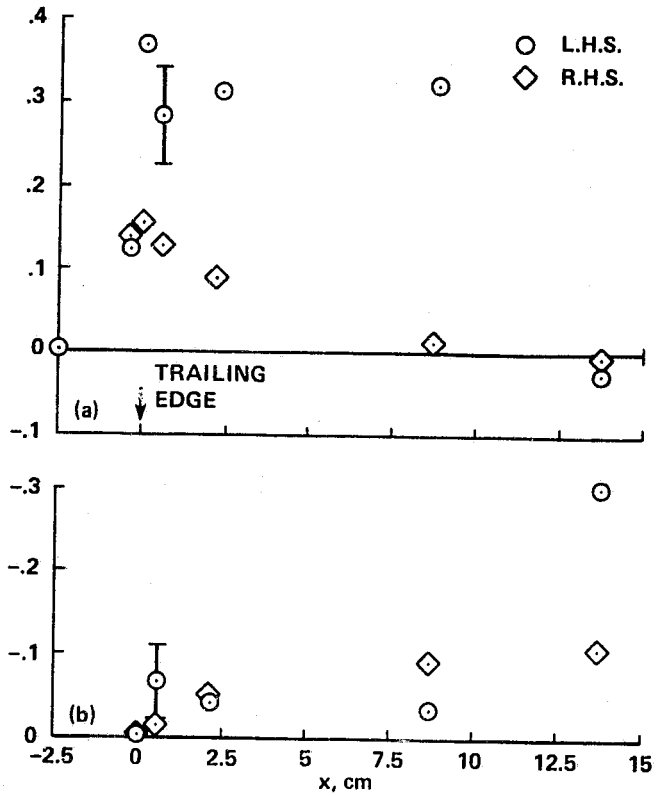

(a) Boundary-layer and wake balance.

(b) Wake balance.

Figure 4.- Momentum-integral balance estimates: $M_n = 0.4$; $Re_L = 24.3 \times 10^6$; $\alpha = 0°$.

ORIGINAL PAGE IS
OF POOR QUALITY

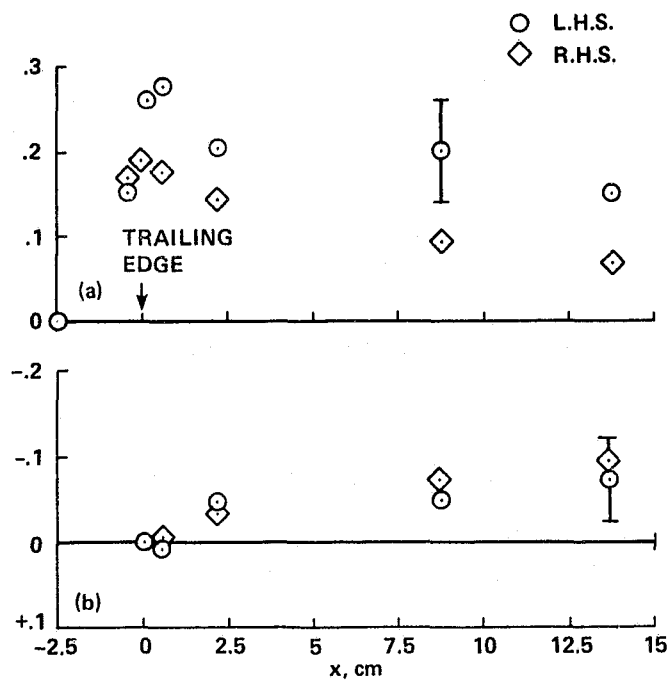

(a) Boundary-layer and wake balance.

(b) Wake balance.

Figure 5.- Momentum-integral balance estimates: $M_n = 0.7$; $Re_L = 36.6 \times 10^6$; $\alpha = 0°$.

ORIGINAL PAGE IS
OF POOR QUALITY

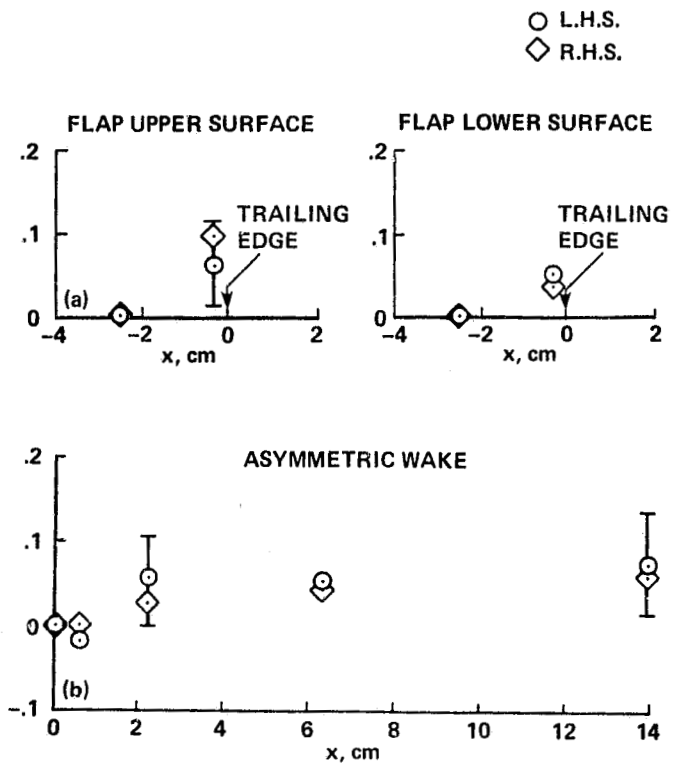

(a) Boundary-layer balance.

(b) Wake balance.

Figure 6.- Momentum-integral balance estimates: M_n = 0.4; Re_L = 24.3×10^6; α = 6.25°.

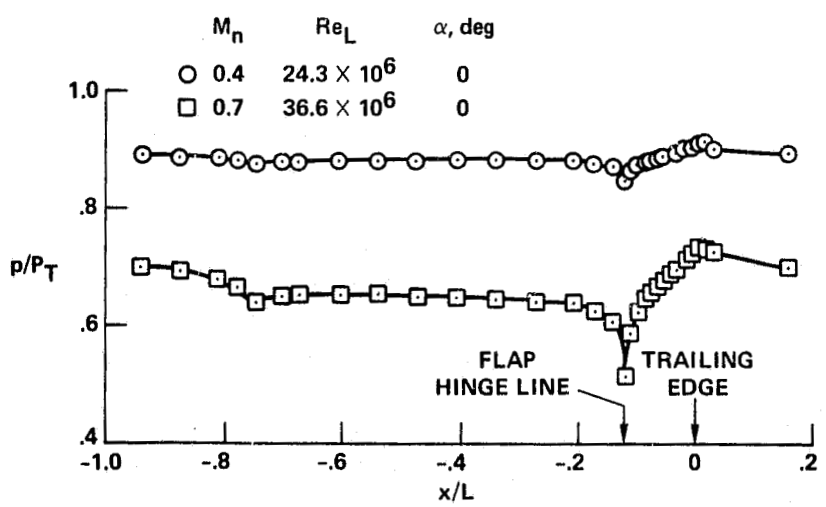

Figure 7.- Static-pressure distributions on the model: α = 0°.

ORIGINAL PAGE IS
OF POOR QUALITY

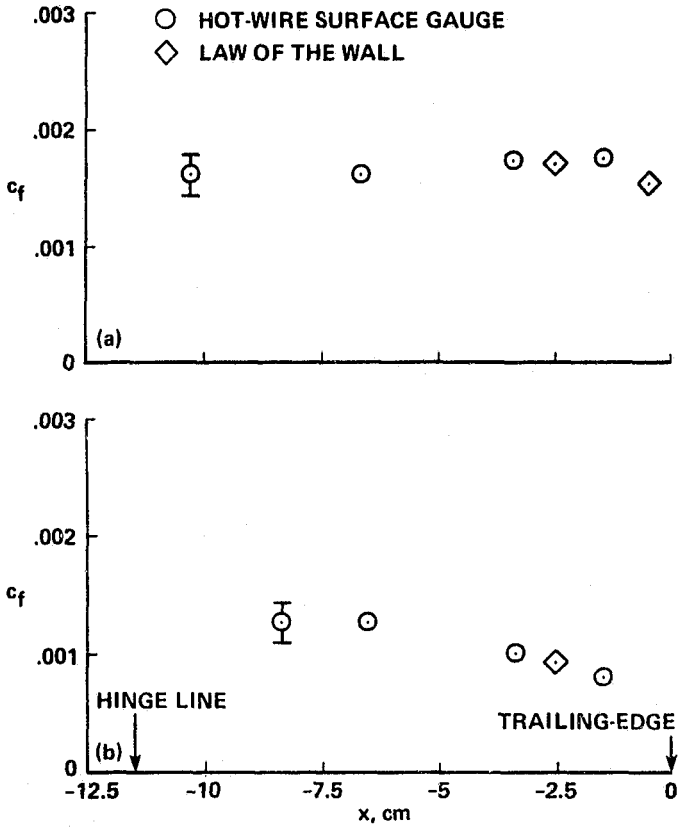

(a) $M_n = 0.4$; $Re_L = 24.3 \times 10^6$.

(b) $M_n = 0.7$; $Re_L = 36.6 \times 10^6$.

Figure 8.- Surface skin-friction distributions: $\alpha = 0°$.

ORIGINAL PAGE IS
OF POOR QUALITY

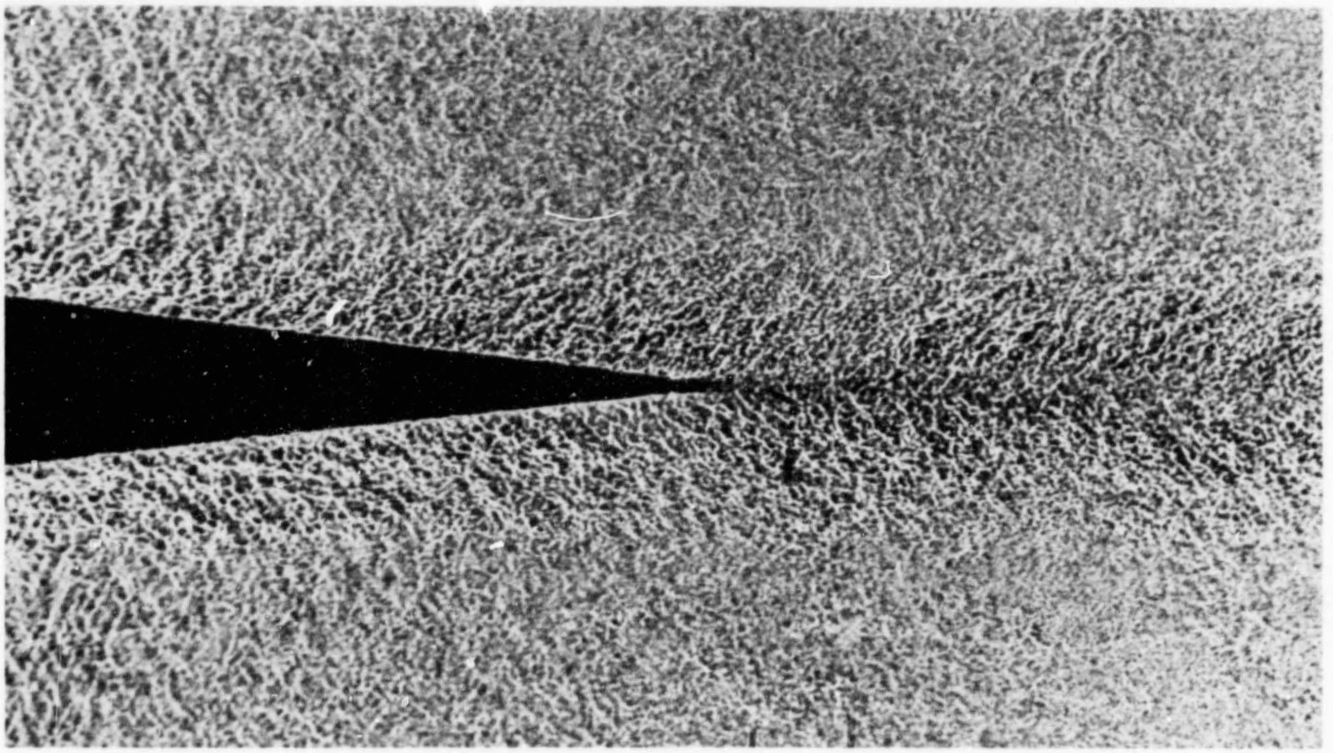

(a) $M_n = 0.7$; $Re_L = 36.6 \times 10^6$.

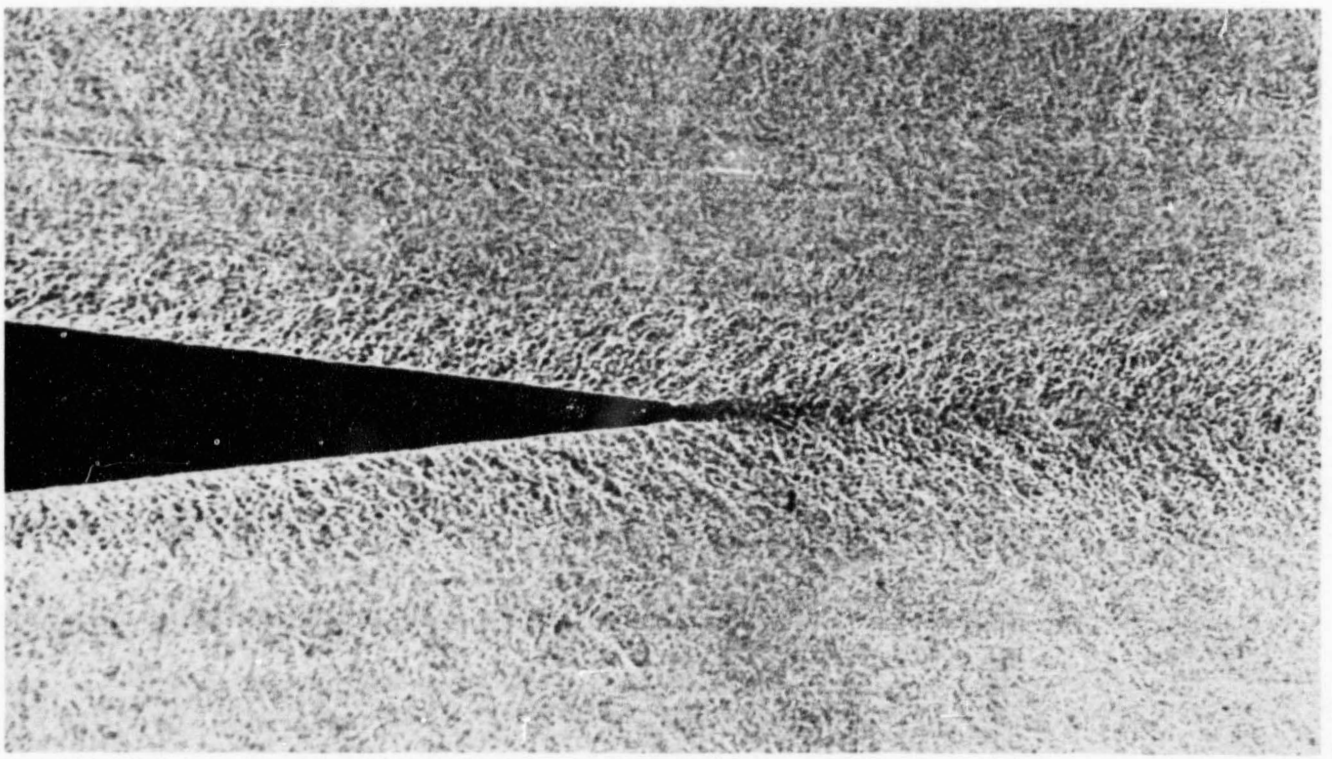

(b) $M_n = 0.4$; $Re_L = 24.3 \times 10^6$.

Figure 9.- Spark shadowgraphs of the flow field: $\alpha = 0°$.

ORIGINAL PAGE

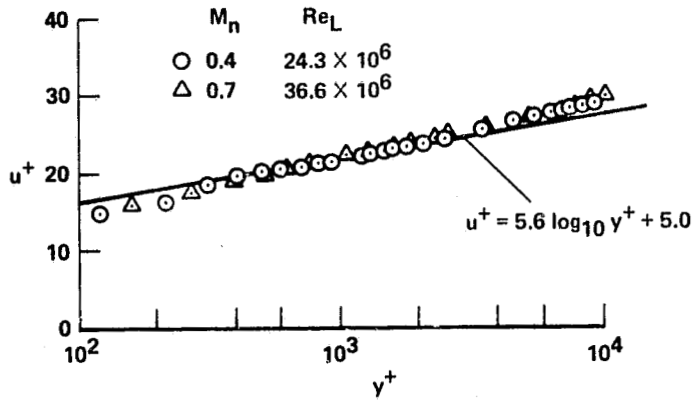

Figure 10.- Flat-plate boundary-layer velocity profiles in law-of-the-wall coordinates.

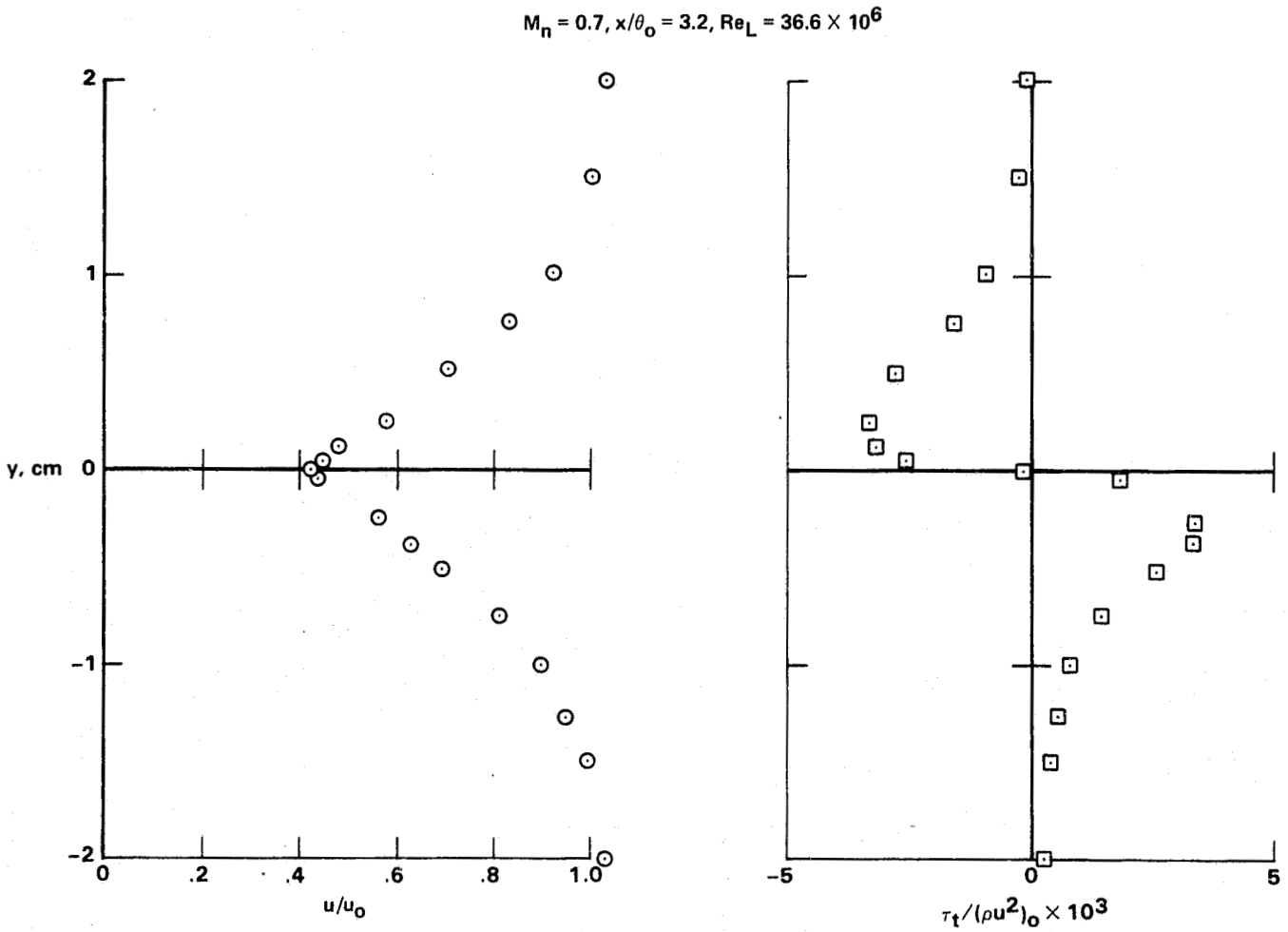

Figure 11.- Mean-velocity and turbulent shear-stress profiles across a symmetric wake: $M_n = 0.7$; $x/\theta_o = 3.2$; $Re_L = 36.6 \times 10^6$.

ORIGINAL PAGE IS
OF POOR QUALITY

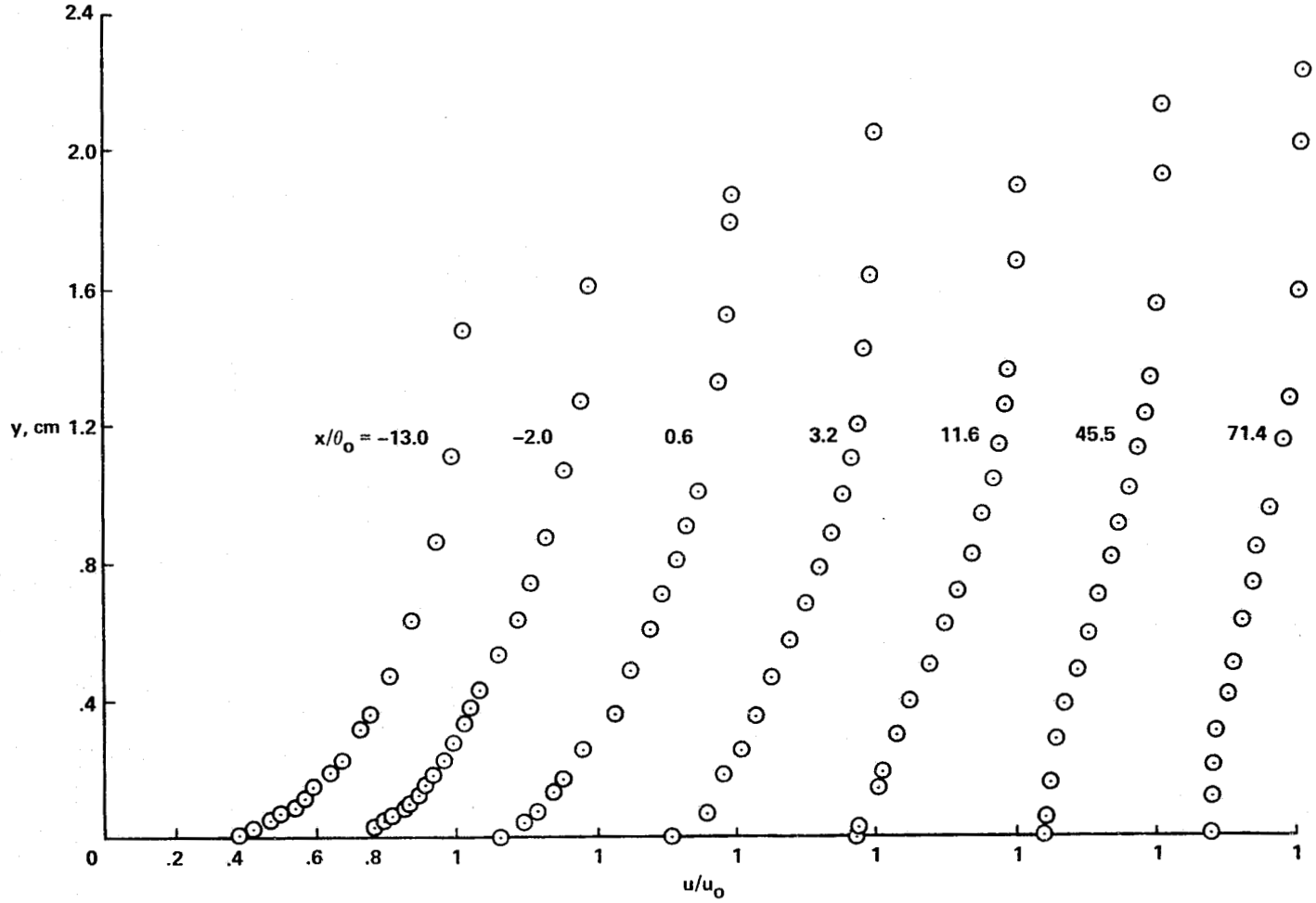

Figure 12.- Mean-velocity profiles in the trailing-edge and near-wake regions: $M_n = 0.7$; $Re_L = 36.6 \times 10^6$; $\alpha = 0°$.

ORIGINAL PAGE IS
OF POOR QUALITY

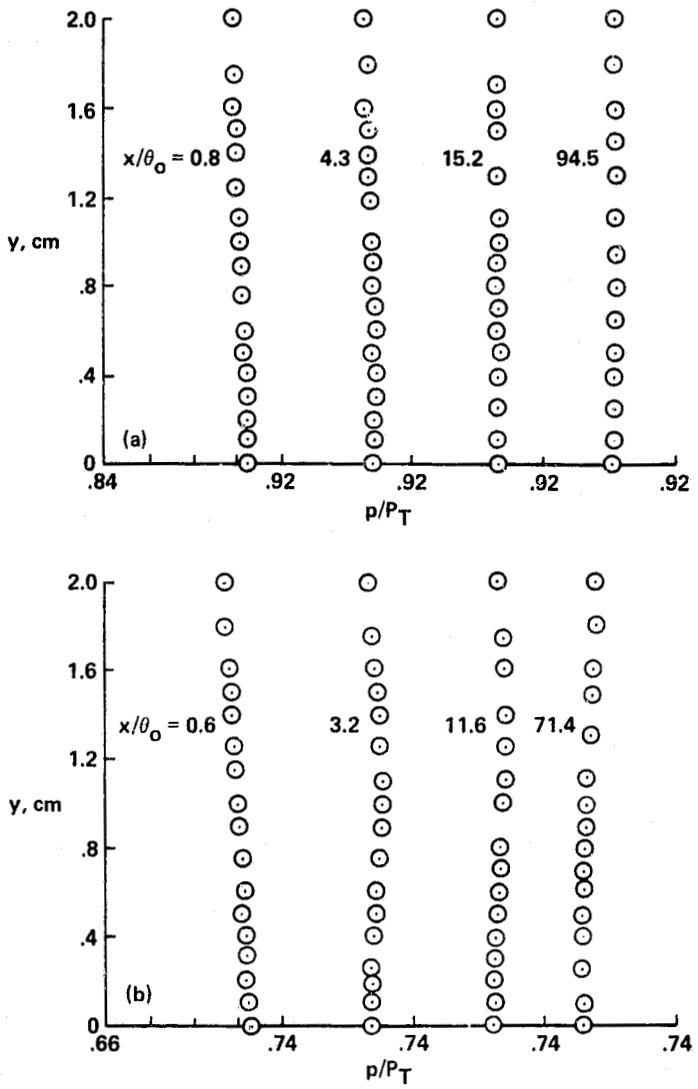

(a) $M_n = 0.4$; $Re_L = 24.3 \times 10^6$.

(b) $M_n = 0.7$; $Re_L = 36.6 \times 10^6$.

Figure 13.- Wake static-pressure profiles: $\alpha = 0°$.

ORIGINAL PAGE IS
OF POOR QUALITY

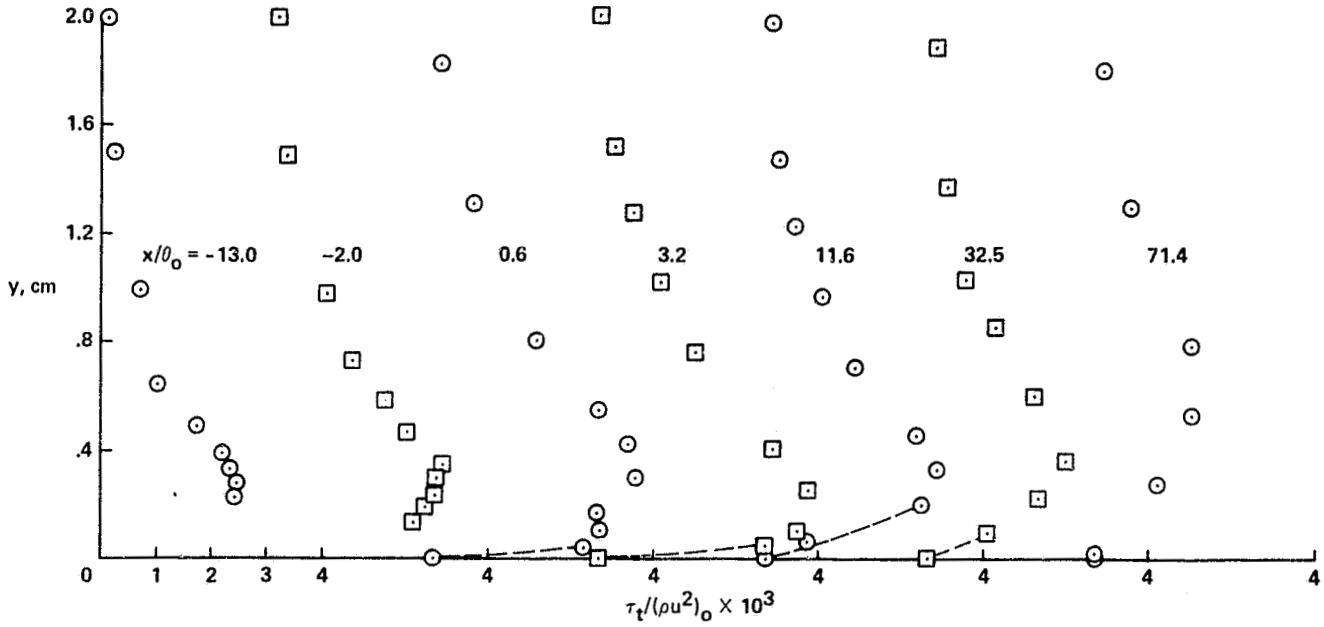

Figure 14.- Turbulent shear-stress profiles in the trailing-edge and near-wake regions: $M_n = 0.7$; $Re_L = 36.6\times10^6$; $\alpha = 0°$.

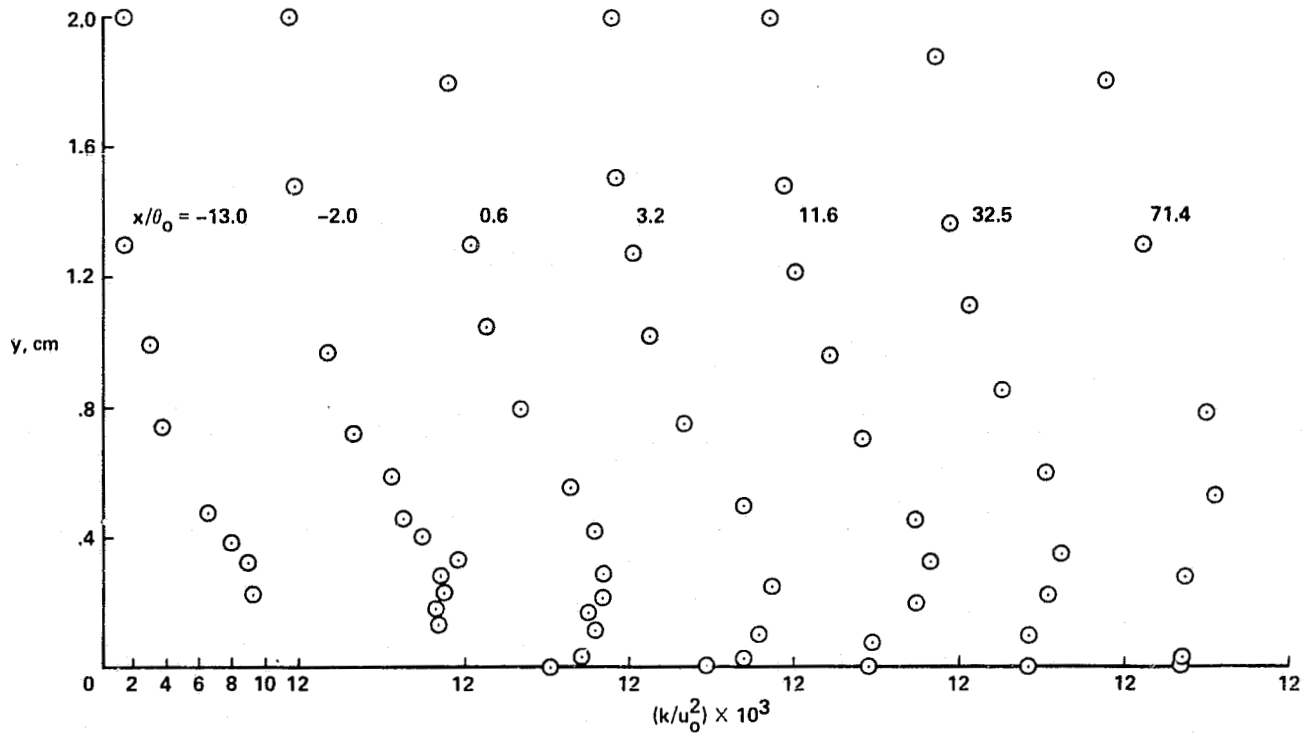

Figure 15.- Turbulent kinetic-energy profiles in the trailing-edge and near-wake regions: $M_n = 0.7$; $Re_L = 36.6\times10^6$; $\alpha = 0°$.

ORIGINAL PAGE IS
OF POOR QUALITY

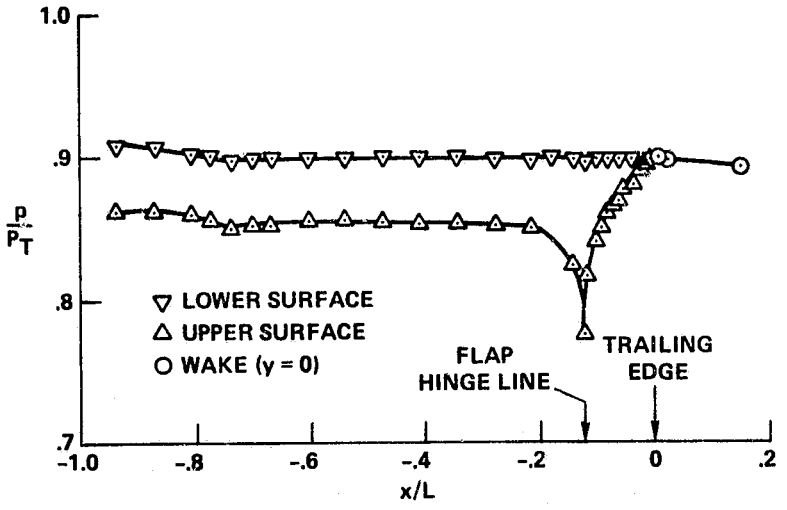

Figure 16.- Model static-pressure distributions: $M_n = 0.4$; $Re_L = 24.3 \times 10^6$; $\alpha = 6.25°$.

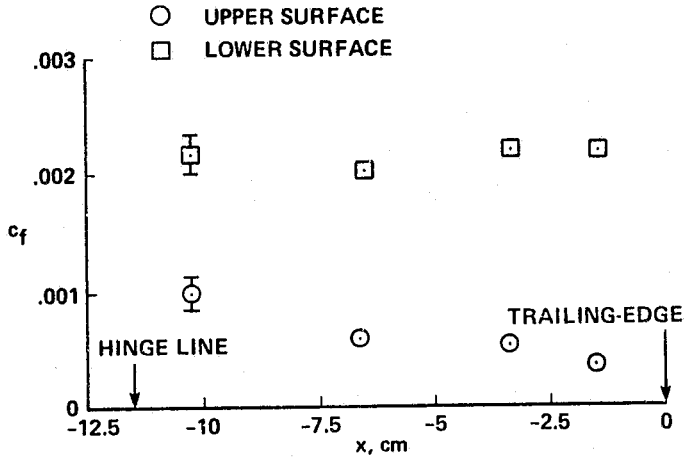

Figure 17.- Surface skin-friction distributions: $M_n = 0.4$; $Re_L = 24.3 \times 10^6$; $\alpha = 6.25°$.

ORIGINAL PAGE IS

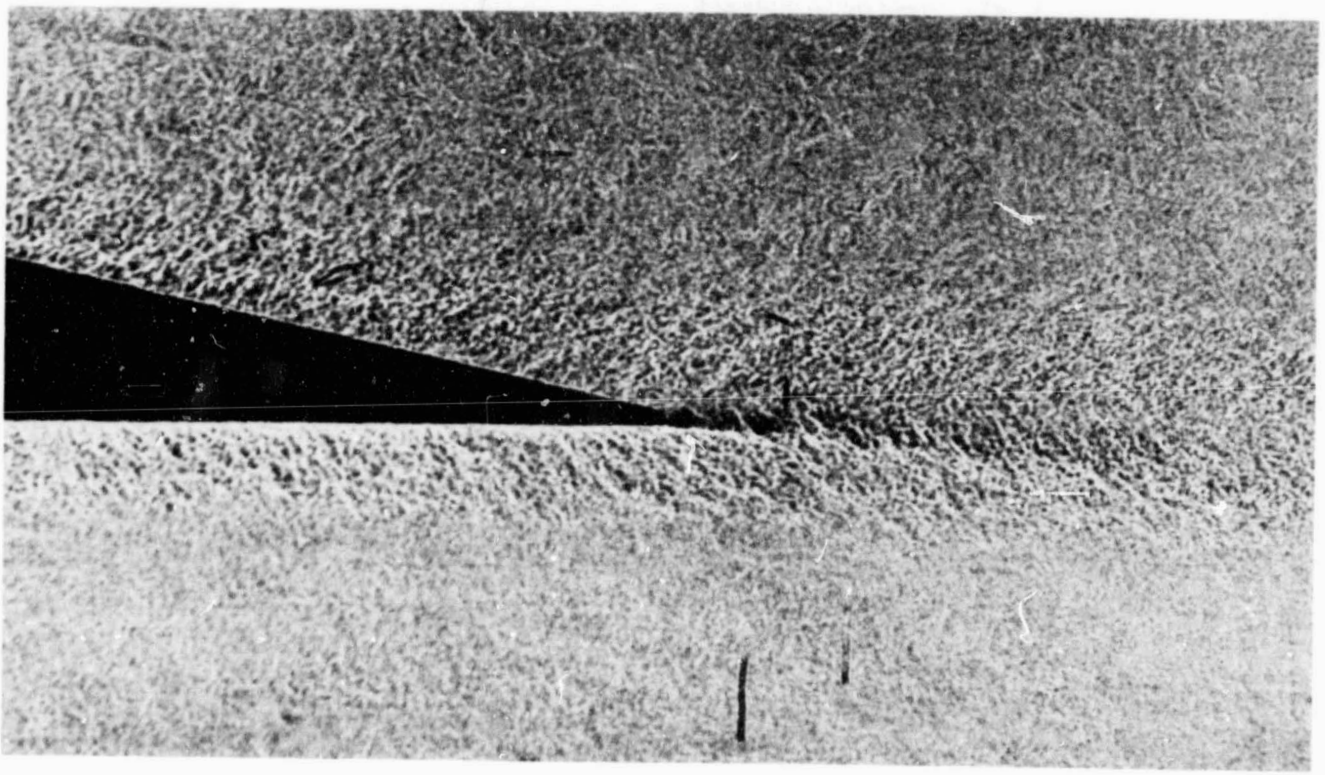

Figure 18.- Spark shadcwgraph of the flow field: $M_n = 0.4$; $Re_L = 24.3 \times 10^6$; $\alpha = 6.25°$.

ORIGINAL PAGE
BLACK AND WHITE PHOTOGRAPH

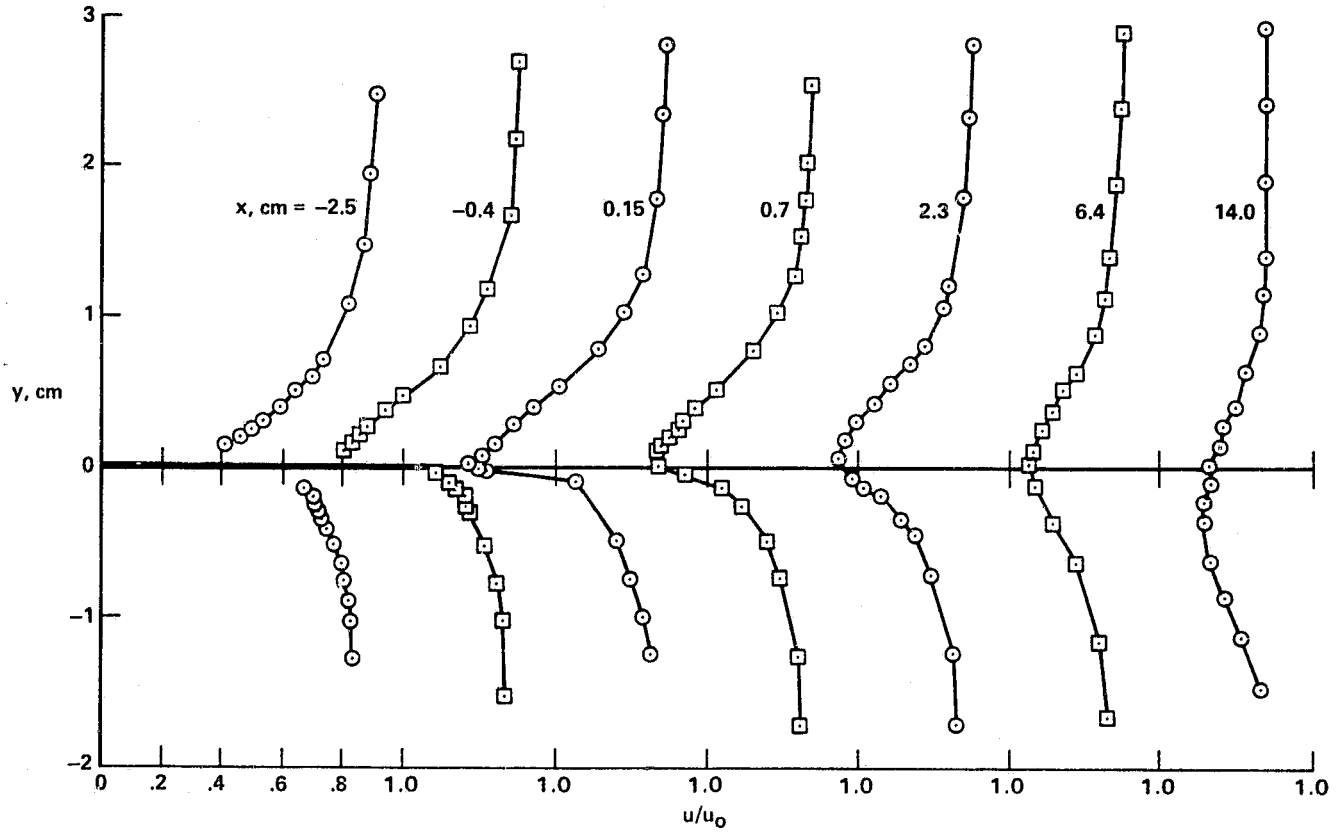

Figure 19.- Mean-velocity profiles in the trailing-edge and near-wake regions: $M_n = 0.4$; $Re_L = 24.3 \times 10^6$; $\alpha = 6.25°$.

ORIGINAL PAGE IS
OF POOR QUALITY

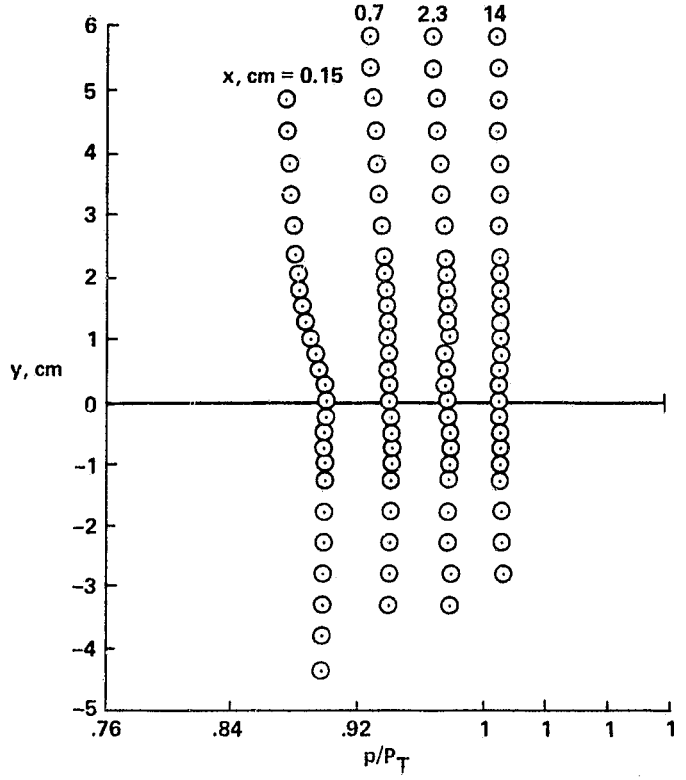

Figure 20.- Wake static-pressure profiles: $M_n \approx 0.4$; $Re_L = 24.3 \times 10^6$; $\alpha = 6.25°$.

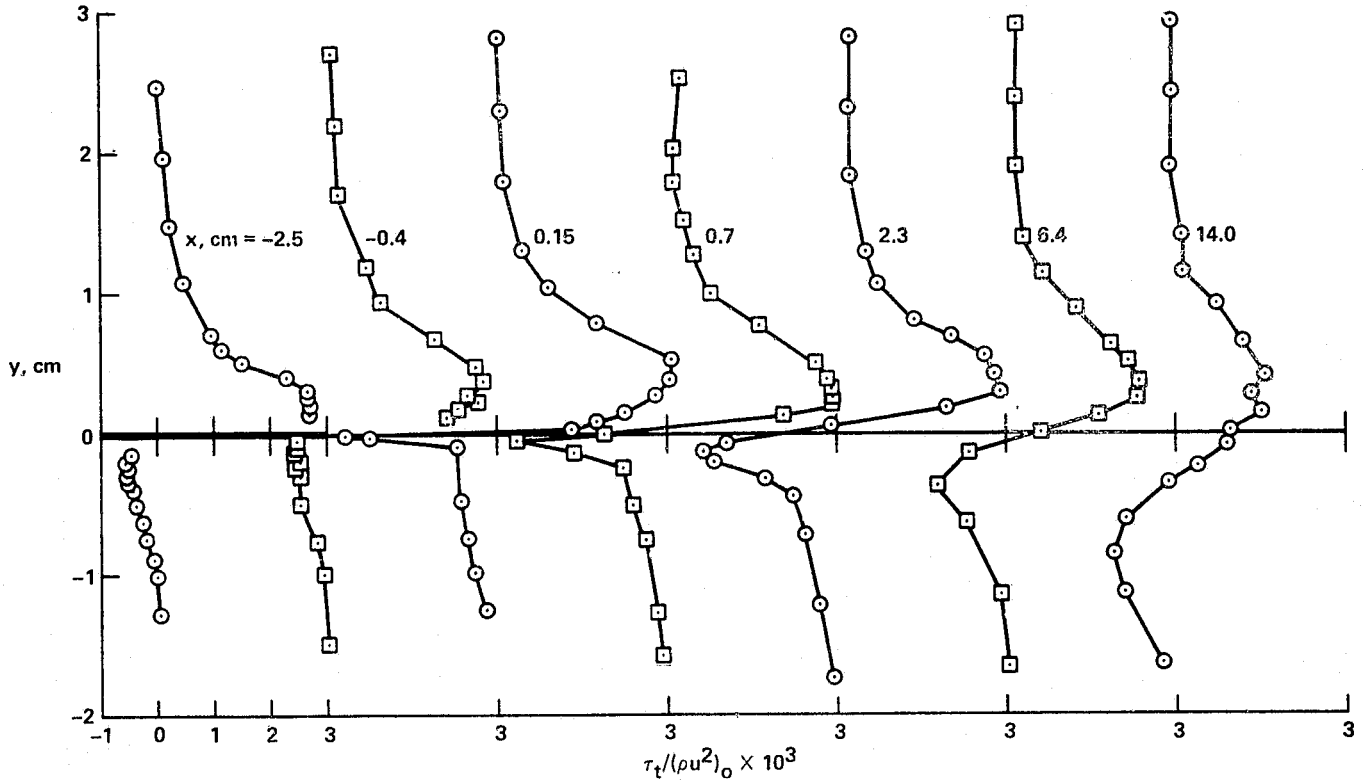

Figure 21.- Turbulent shear-stress profiles in the trailing-edge and near-wake regions: $M_n = 0.4$; $Re_L = 24.3 \times 10^6$; $\alpha = 6.25°$.

ORIGINAL PAGE IS

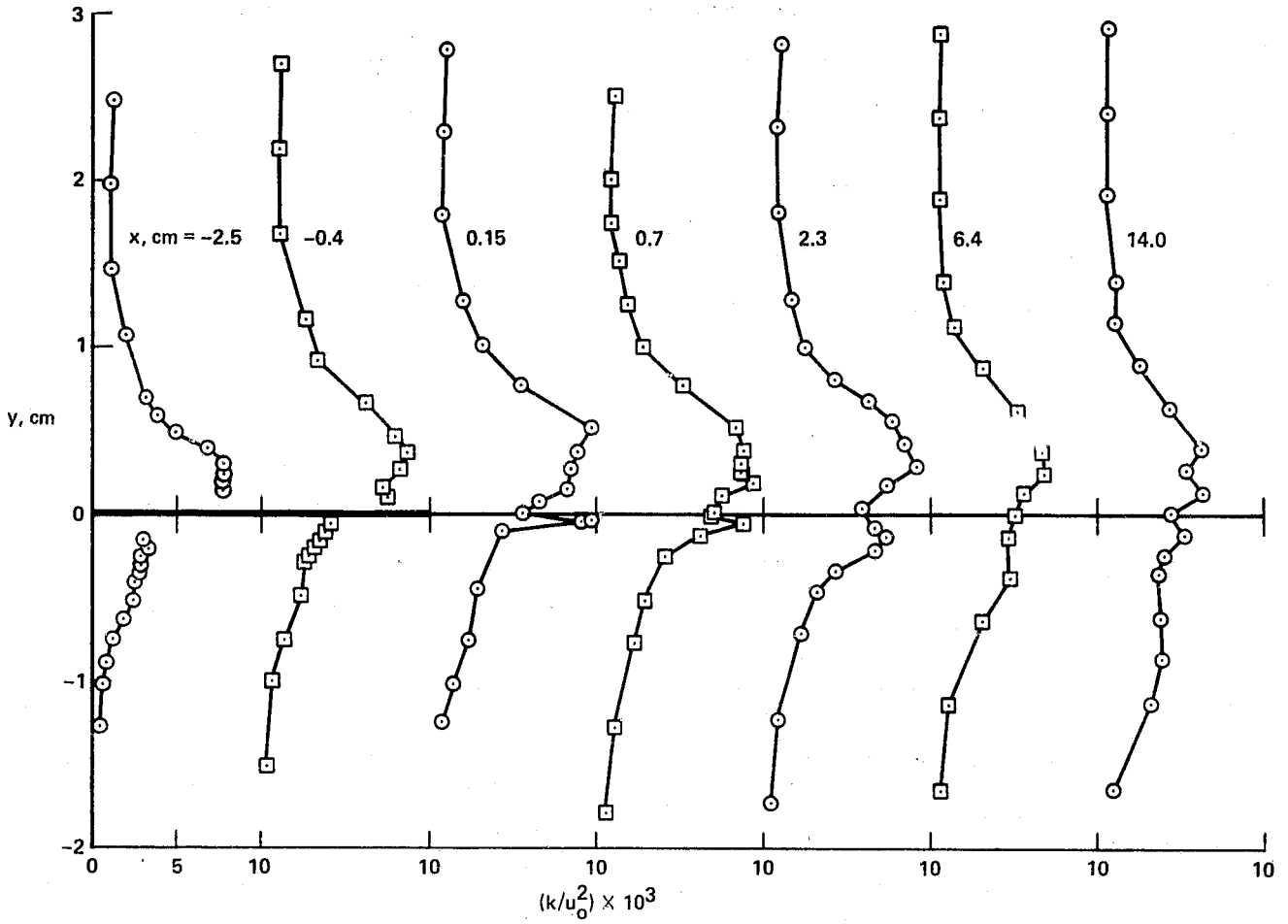

Figure 22.- Turbulent kinetic energy profiles in the trailing-edge and near-wake regions: $M_n = 0.4$; $Re_L = 24.3 \times 10^6$; $\alpha = 6.25°$.

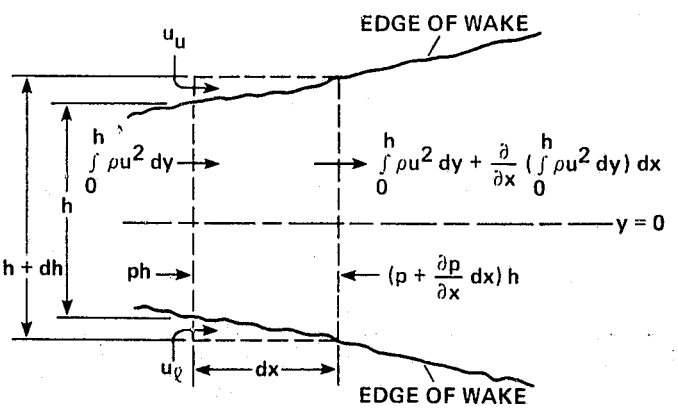

Figure 23.- Sketch defining notation for deriving wake momentum integral equation.

ORIGINAL PAGE IS
OF POOR QUALITY

1. Report No.	2. Government Accession No.	3. Recipient's Catalog No.
NASA TM-84375		

4. Title and Subtitle	5. Report Date
AN EXPERIMENTAL DOCUMENTATION OF TRAILING-EDGE FLOWS AT HIGH REYNOLDS NUMBERS	August 1983
	6. Performing Organization Code
7. Author(s) P. R. Viswanath (Joint Institute for Aeronautics and Acoustics, Stanford University, Stanford, California), J. W. Cleary, and H. L. Seegmiller	8. Performing Organization Report No. A-9376
9. Performing Organization Name and Address NASA Ames Research Center Moffett Field, Calif. 94035	10. Work Unit No. T-6459
	11. Contract or Grant No.
12. Sponsoring Agency Name and Address National Aeronautics and Space Administration Washington, D.C. 20546	13. Type of Report and Period Covered Technical Memorandum
	14. Sponsoring Agency Code 505-31-01

15. Supplementary Notes

Point of Contact: H. L. Seegmiller, Ames Research Center, M/S 229-1, Moffett Field, Calif., 94035. (415)965-6211 or FTS 448-6211

16. Abstract

Experiments documenting attached trailing-edge and near-wake flows at high Reynolds numbers are described. A long, airfoil-like model was tested at subsonic and low transonic Mach numbers, and both symmetrical and asymmetrical flows with pressure gradients upstream of the trailing edge were investigated. Model surface pressures and detailed mean and turbulence flow qualities were measured in the vicinity of the trailing edge and in the near-wake. The data obtained are presented mostly in tabular form; they are of sufficient quality and detail to be useful as test cases in assessing turbulence models and calculation methods.

17. Key Words (Suggested by Author(s))	18. Distribution Statement
Turbulent boundary layer Turbulent wake Laser Doppler velocimeter	Unlimited Subject Category - 34

19. Security Classif. (of this report)	20. Security Classif. (of this page)	21. No. of Pages	22. Price*
Unclassified	Unclassified	48	A03

*For sale by the National Technical Information Service, Springfield, Virginia 22161